JOURNAL OF COMPUTATIONAL PHYSICS 101, 25–50 (1992)

Shadowing and Iterative Interpolation for Čebyšev Mixing Transformations

D. GAVELEK

Department of Physics, Illinois Institute of Technology, Chicago, Illinois 60616

AND

T. ERBER

Department of Physics and Department of Mathematics, Illinois Institute of Technology, Chicago, Illinois 60616

Received October 30, 1990

The iteration of Čebyšev polynomials generates mixing transformations that model canonical features of chaotic systems: These include pseudo-random evolution, ergodicity, fading memory, and the irreversible dispersal of any set of positive measure throughout the mixing region. Mixing processes are also analytically and numerically unstable. Nevertheless, iterative interpolation, or numerical retrodiction, demonstrates that the computer generated trajectories are shadowed within strict error bounds by exact Čebyšev iterates. Pervasive shadowing is, however, not sufficient to ensure a generic correspondence between computer simulations and "true dynamics." This latitude is illustrated by several basic distinctions between the computer generated orbit structures and the exact analytic orbits of the Čebyšev mixing transformations.

CONTENTS

1. INTRODUCTION

1.1. Dynamical Instability and Shadowing

The description of chaotic systems involves two seemingly contradictory requirements. On the one hand, the dynamical systems that are used to model stochastic processes such as the mixing of cocoa in milk must be very sensitive to small variations in the initial conditions or other perturbations; but at the same time the correspondence between the dynamical systems and computer simulations must be sufficiently robust so that numerical results can be meaningfully compared with theoretical predictions. Simply put, the evolution of these systems must appear to be dynamically unstable as well as numerically stable. Anosov [1], Bowen [2], and Hammel, Yorke, and Grebogi [3, 4] have shown that these nominally antithetic stability criteria can be reconciled for a wide class of dynamical systems by the construction of shadowing trajectories—that is, iterative sequences of the exact dynamics that follow the computer generated values within strict error bounds. In the present work these results are extended to the "fully developed chaos" that is generated by iterating the logistic map

$$x_n \to f_L(x_n) = a x_n (1 - x_n) = x_{n+1} \tag{1.1}$$

when $a = 4$ and $0 \leqslant x_n \leqslant 1$ [5, 6]. Since, in this case, Eq. (1.1), is conjugate to the quadratic Čebyšev polynomial, whose analytic and computer generated orbit structures are known [7–11], the shadowing sequences can be constructed explicitly by iterative interpolation. These methods can be used to verify that all of the computer orbits of (1.1) are in fact shadowed by exact Čebyšev iterates.

However, these strong shadowing properties do not

0021-9991/92 $5.00

guarantee that there is a generic correspondence between the computer simulations and the exact orbit structure of the Čebyšev mixing transformations. The discrete and finite nature of machine computations imposes a number of unavoidable restrictions on the numerical orbits. First of all, in contrast to the analytic Čebyšev iterations, which generally extend indefinitely far into the "past" and the "future," the computer sequences are all strictly limited in length: they begin at points that do not have any pre-images in the set of accessible computer numbers; and they end by merging into terminal cycles. Numerical divergences are suppressed. Furthermore, while all of the denumerably infinite cycles of the Čebyšev iterates are repulsive, the computer generated terminal cycles are all embedded in attractor basins. The pseudo-random character of the computer sequences also implies that the orbits associated with these attractors have specific statistical attributes. For instance, about 80% of all the computer numbers are part of a single dominant orbit [10], and approximately 65% of the iteration sequences contained in this dominant orbit enter the terminal loop through a single point [11–13].

All of these combinatorial properties of the computer generated orbits are reflected in the associated set of shadowing trajectories: But these, in turn, are only a finite fragment of the exact Čebyšev orbits—these include uncountably many acyclic orbits each with a countably infinite number of elements, as well as a countably infinite number of cyclic orbits each with a countably infinite number of elements [9]. Clearly, the existence of shadowing trajectories cannot bridge the gap between machine computations and infinite processes. Nevertheless shadowing is a useful means for checking the fidelity of the machine simulations of chaotic systems and furnishes some justification for the empirical agreement between statistical properties derived from computer experiments and theoretical predictions [8, 14].

In Sections 1.2–1.6 we briefly review the connections between stability and approximation criteria in classical and abstract dynamics. The emphasis throughout is on the physical background of the abstract stability and shadowing concepts. This orientation will turn out to be helpful in following the winding trail of mathematical theorems, plausibility arguments, and computer verifications that leads from abstract shadowing to machine simulations.

1.2. Stability and Approximation Criteria in Classical Dynamics

The construction of shadowing trajectories generally requires a combination of methods drawn from dynamical systems theory, numerical analysis, and computer programming. Each of these components involves distinct criteria for approximating or comparing one trajectory with another, and this formal diversity makes it possible for dynamical instability to coexist with robust numerical approximations. The simplest illustration of these options occurs in the classical theory of dynamical stability. Specifically, let $z(t, p)$ be the solution of a problem in Newtonian mechanics where t is the time, and $p = \{p_j, j = 1, ..., N\}$ denotes a set of parameters representing constraints and boundary conditions. Suppose further that all the physically relevant values of the p_j's span some parameter space, and that there is a particular point p_0 in this space associated with the unperturbed trajectory $z(t, p_0)$. Then if p denotes any other point in a neighborhood S of p_0, the corresponding trajectory $z(t, p)$ will describe a perturbed motion. The basic Liapunov stability criterion then asserts that the unperturbed trajectory $z(t, p_0)$ is stable with respect to variations of p in the parameter set S if for each $\varepsilon > 0$ there is a $\delta > 0$ such that the inequality

$$|z(t_0, p_0) - z(t_0, p)| < \delta \tag{1.2a}$$

implies

$$|z(t, p_0) - z(t, p)| < \varepsilon \tag{1.2b}$$

for some time interval $t > t_0$, [15, 16]. Geometrically this simply means that the perturbed and unperturbed trajectories track each other within the hypercylinder (1.2b), if the base or cross section cut by the plane $t = t_0$, at the initial instant, i.e., (1.2a), is sufficiently small.

Suppose now that for convenience in numerical evaluation $z(t, p_0)$ is approximated by an interpolation polynomial. In the simplest case of Lagrange interpolation over the set $t_0 < \cdots < t_j < \cdots < t_n$, this means that $z(t, p_0)$ is represented by

$$z(t, p_0) = \sum_{j=0}^{n} l_j(t)\, z(t_j, p_0) + R_n(t, p_0), \tag{1.3a}$$

where

$$l_j(t) = \frac{(t - t_0) \cdots (t - t_{j-1})(t - t_{j+1}) \cdots (t - t_n)}{(t_j - t_0) \cdots (t_j - t_{j-1})(t_j - t_{j+1}) \cdots (t_j - t_n)} \tag{1.3b}$$

and the remainder term is bounded by

$$|R_n(t, p_0)| \leqslant \frac{(t_n - t_0)^{n+1}}{(n+1)!} \operatorname*{Max}_{t_0 \leqslant t \leqslant t_n} \left| \frac{\partial^{n+1} z(t, p_0)}{\partial t^{n+1}} \right|. \tag{1.3c}$$

Clearly, if the time dependence of $z(t, p_0)$ is sufficiently smooth so that the derivative bounds in (1.3c) ensure small error estimates, polynomial interpolation can be numerically useful. Since this condition is independent of the nature of the variation of $z(t_0, p)$ with respect to the parameter set

p_j, it is in principle possible to construct polynomial approximations for the unperturbed motion $z(t, p_0)$, even if this trajectory is dynamically unstable.

1.3. Stability and Instability Criteria for Anosov Diffeomorphisms

Approximate representations of unstable dynamics are utilized in practice for modeling non-linear oscillators and other systems that have chaotic vibrations and a sensitive dependence on initial conditions [17]. In these cases, neighboring trajectories do not remain clustered together, as presumed in (1.2b), but rather spread out rapidly throughout the accessible phase space. This dispersive property can also be used to characterize instability in abstract dynamical systems such as Anosov diffeomorphisms. In this formalism the evolution of a system through a set of states, $x_0, x_1, ..., x_j$, is described by the iteration of a mapping, i.e.,

$$\begin{array}{ccccccc} x_0 & \longrightarrow & x_1 & \longrightarrow & x_2 & \longrightarrow \cdots \longrightarrow & x_j; \\ & & \updownarrow & & \updownarrow & & \updownarrow \\ x_0 & \longrightarrow & f(x_0) & \longrightarrow & f^2(x_0) & \longrightarrow \cdots \longrightarrow & f^j(x_0). \end{array} \tag{1.4a, 1.4b}$$

In analogy with the Γ-space of classical statistical mechanics, the x_j's specify the complete configuration of the system. For simplicity, we will assume that this configuration space M, is an open subset of m-dimensional Euclidean space $\mathbb{R}^m$. The corresponding m-component mappings do not have to be derivable from any Hamiltonian, although indirect mechanical constructions may be possible [18].

The clustering and dispersion of trajectories in this iterative scheme can be characterized by straightforward generalizations of the corresponding notions in classical dynamics. The simplest classical prototype is the saddle shaped electric potential of a Penning trap [19]. In practice, this hyperbolic energy surface can be set up by applying opposing voltages to orthogonal pairs of hyperbolically shaped electrodes. In this case the Jacobian of the potential reduces to the gradient; and this, in turn, indicates the directions of bounded and unbounded oscillations when a charged particle is inserted into the trap [20].

In the abstract version of the theory the scalar potential is replaced by the m-component mapping f. The generalization of the gradient criterion for bounded or unbounded oscillations is then expressed in terms of the action of the Jacobian in contracting or expanding vectors in the systems' configuration space. Specifically, let $Df(x)$ denote the $m \times m$ Jacobian matrix of first partial derivatives of the components of f at the point x. Then if ξ is a vector in $\mathbb{R}^m$, the matrix product, $Df(x)\xi$, is a linear transformation that generally alters the length of ξ. In particular, if $\|Df(x)\xi\| < \|\xi\|$, where the double bars denote the norm, the vector ξ is contracted for f at x. Similarly, if $\|Df(x)\zeta\| > \|\zeta\|$, then ζ is an expanding vector for f at x. In analogy with the Penning trap example, a point x is said to be hyperbolic if every associated Jacobian vector transformation can be represented in terms of contracting and expanding vectors at x.

These intuitively plausible notions can now be extended by introducing some additional structure [1, 21]:

(1) If f is a diffeomorphism, i.e., both f and its inverse f^{-1} are continuously differentiable, then the sequence of states (1.4b) can evolve forwards (f^j) as well as backwards (f^{-j}); this is the iterative counterpart of time reversible motion.

(2) The general stability criterion for these systems can then be expressed in terms of a uniform contraction condition: A vector $\xi \in \mathbb{R}^M$ is a *contracting* or *stable* vector for f at x if there are positive constants c and $\lambda < 1$, such that

$$\|Df^j(x)\xi\| \leqslant c\lambda^j \|\xi\| \qquad \text{for all} \quad j \geqslant 0. \tag{1.5}$$

If the evolution index j is identified with discrete time increments, then (1.5) is an iterative analogue of the Liapunov criterion (1.2b).

(3) Instability, or the dispersion of trajectories, can be described by a complementary condition: A vector $\zeta \in \mathbb{R}^m$ is an *expanding* or *unstable* vector for f at x if there are positive constants $\bar{c}$ *and* $\bar{\lambda}$, such that

$$\|Df^j(x)\zeta\| \geqslant \bar{c}\bar{\lambda}^j \|\zeta\| \qquad \text{for all} \quad j \geqslant 0. \tag{1.6}$$

Since f is a diffeomorphism, (1.6) is also equivalent to a contraction condition for successive pre-images of f, i.e.,

$$\|Df^{-j}(x)\zeta\| \leqslant c\lambda^j \|\zeta\| \qquad \text{for all} \quad j \geqslant 0. \tag{1.7}$$

The inverse relation of (1.6) and (1.7) has an obvious analogue in classical dynamics—running the film of a dispersing water spray backwards yields the images of a convergent implosion. It will become apparent in Sections 1.5 and 1.6 that "inverse" stability criteria such as (1.7) are the key to the construction of shadowing trajectories.

(4) Since Anosov diffeomorphisms are intended to illustrate the behavior of chaotic systems, it is desirable to eliminate trajectories that correspond to smooth and incompressible laminar flows. This can be done by strengthening the conditions associated with hyperbolic points. Specifically, for a given diffeomorphism f and a particular point x, let $E^{\text{st}}(x)$ denote the linear subspace of $\mathbb{R}^m$ spanned by all the contracting vectors satisfying (1.5). Furthermore, let $E^{\text{un}}(x)$ be the linear subspace of $\mathbb{R}^m$

spanned by all the unstable or expanding vectors satisfying (1.6). Then x is a *hyperbolic point* if

$$E^{st}(x) \oplus E^{un}(x) = \mathbb{R}^m. \tag{1.8}$$

In analogy with the Penning trap dynamics, this condition ensures that all the trajectories passing through x either condense or disperse; parallel flow or neutral equilibrium is excluded.

(5) The essential content of this abstract dynamics can now be summarized in the definition of a *hyperbolic set* [21]: A set $\Lambda \subset M$, where M is the configuration space of the system, is a uniform hyperbolic set for f if Λ is compact, invariant under the action of f, i.e., $f\Lambda = \Lambda$, and if every point $x \in \Lambda$ is hyperbolic. This means that there are positive constants c and $\lambda < 1$, independent of x, such that

$$\|Df^j(x)\xi\| \leqslant c\lambda^j \|\xi\|, \quad \forall x \in \Lambda, \xi \in E^{st}(x), j \geqslant 0; \tag{1.9a}$$

$$\|Df^{-j}(x)\zeta\| \leqslant c\lambda^j \|\zeta\|, \quad \forall x \in \Lambda, \zeta \in E^{un}(x), j \geqslant 0. \tag{1.9b}$$

The stability condition (1.9a) and the instability condition (1.9b) are obvious extensions of (1.5) and (1.7).

Finally, if the entire configuration space M is a hyperbolic set for f, then f is said to be an *Anosov diffeomorphism.*

1.4. Approximation Criteria for Anosov Diffeomorphisms: Structural Stability and Shadowing

Chaotic evolution and robust approximation are compatible for Anosov diffeomorphisms because these systems are both *dynamically unstable* as well as *structurally stable.* According to Eqs. (1.6), (1.7), and (1.9b), dynamical instability merely requires a local dispersion of neighboring trajectories. In contrast, structural stability refers to the global response of the entire set of iterative sequences (1.4b) if the diffeomorphism f is shifted. Physically, this corresponds to changing the dynamics of particles in a Penning trap by modifying the electrodes or altering the applied voltages. Suppose, in particular, that f and g are two Anosov diffeomorphisms associated with the configuration space M, where g is obtained by a small perturbation of f. Technically this means that f is close to g in the C^1 topology, or that f and g, as well as their first derivatives, differ only slightly [22]. Under these circumstances, the orbits of f are isomorphically mapped onto the orbits of g by the conjugacy transform

$$g = h \circ f \circ h^{-1}, \tag{1.10}$$

where h is a homeomorphism close to the identity function in the C^0 topology [21, 23].

Structural stability is an extremely restrictive condition. It implies that the iterative properties of the trajectories in (1.4b)—including the attraction or repulsion of cycles—are preserved under small perturbations of f. Consequently, even if the individual iterations in (1.4b) are perturbed so as to cause large cumulative shifts of the configurations x_j, structural stability ensures that these deviations do not alter the global dynamics generated by f. The approximations introduced by "stabilized perturbations" of this type can be described by means of *pseudo-trajectories* and *shadowing trajectories.*

A pseudo-trajectory of f is obtained from an exact trajectory such as (1.4a), (1.4b)

$$x_0 \to f(x_0) \to f(x_1) \to \cdots \to f(x_j) \to \cdots \tag{1.11}$$

by inserting step-wise perturbations δ_j between each iteration, i.e.,

$$\begin{array}{ccccccccc} x_0 + \delta_0 & \to & f(x_0') + \delta_1 & \to & f(x_1') + \delta_2 & \to \cdots \to & f(x_{j-1}') + \delta_j & \to \cdots & \text{(1.12a)} \\ \updownarrow & & \updownarrow & & \updownarrow & & \updownarrow & & \\ x_0' & \longrightarrow & x_1' & \longrightarrow & x_2' & \longrightarrow \cdots \longrightarrow & x_j' & \longrightarrow \cdots & \text{(1.12b)} \end{array}$$

If the exact trajectory $\{x_j\}$ is dynamically unstable then generally it will not be followed by the pseudo-trajectory $\{x_j'\}$. In fact, if d is a metric on the configuration space M, then the only restriction on the distance between x_j and x_j' is that

$$\operatorname*{Max}_{0 \leqslant j \leqslant N} \{d(x_j, x_j')\} \leqslant \operatorname{diam} M, \tag{1.13a}$$

where the diameter of M is given by

$$\operatorname{diam} M = \sup\{d(p, q) \mid p, q \in M\}. \tag{1.13b}$$

Nevertheless, the wandering of the pseudo-trajectory $\{x_j'\}$ is severely constrained by the structural stability of f.

To be precise, suppose that every one of the individual perturbations δ_j in (1.12a) is limited by a fixed bound δ, i.e.,

$$d(f(x_{j-1}'), x_j') < \delta, \qquad 0 \leqslant j \leqslant N. \tag{1.14}$$

Such bounded, step-wise perturbations are said to generate δ pseudo-trajectories. Then the order imposed by structural stability is expressed by the

SHADOWING THEOREM OF ANOSOV [1] AND BOWEN [2]. *Suppose that f is an Anosov diffeomorphism over M, and that $\{x_j'\}$ is a δ pseudo-trajectory derived from the exact*

trajectory $\{x_j\}$. *Then there exists at least one other exact trajectory* $\{y_j\}$ *in M generated by*

$$y_0 \to f(y_0) \to f(y_1) \to \cdots \to f(y_j) \to \cdots, \quad (1.15)$$

that approximates or shadows *the pseudo-trajectory within a precision* $\varepsilon > 0$, *i.e.*,

$$d(f(y_{j-1}), x'_j) < \varepsilon \quad (1.16)$$

for all $0 \leqslant j \leqslant N$, *and sufficiently small* $\delta > 0$.

The exact sense in which chaotic evolution and robust approximation coexist for Anosov diffeomorphisms can now finally be summarized by the interrelation of three sequences: If $\{x_j\}$ is an exact but unstable trajectory of f, then the perturbed δ pseudo-trajectory $\{x'_j\}$ will progressively deviate from $\{x_j\}$ for increasing j. However, the wandering of the pseudo-trajectory is not arbitrary because there is at least one other exact trajectory $\{y_j\}$ of f that approximates or shadows $\{x'_j\}$ within strict error bounds.

1.5. Shadowing in Computer Simulations of Unstable Systems

At first sight it seems plausible to identify the perturbations δ_j in (1.12a) with the roundoff and truncation errors that occur in computer simulations. In particular, if a device is programmed to generate the unstable trajectories of an Anosov system, it is tempting to argue that the shadowing theorem ensures that the simulations cannot possibly go wrong—the effect of roundoff is simply to shift the computed sequence of values from the vicinity of one exact trajectory to the proximity of another exact trajectory [14]. Unfortunately this argument is flawed because the analytic orbits and computer trajectories are not in one-to-one correspondence as stipulated in (1.10) [24]. Nevertheless, empirical evidence for shadowing can be inferred from computer simulations of chaotic systems [25, 26, 9, 14]. For example, in a mixing process on an interval the values of the iterates $\{x_j\}$ and $\{y_j\}$ are usually so thoroughly dispersed that eventually their relative distribution becomes *independent* of the starting points x_0 and y_0 (fading memory!). The statistical properties of these distributions are determined by the probabilistic metric spaces associated with the mixing processes [27]. In particular cases these distributions can be obtained explicitly and compared with the results of computer experiments. The agreement turns out to be uniformly excellent even though the statistical computer results are obtained from iterations extending into the millions, while the numerical accuracy of an individual element x_j is completely obliterated by roundoff after only 50 iterations [8]!

Another striking trend of the computer simulations is that consistent statistical results can be obtained from iterations of the Hénon map, which is not uniformly hyperbolic [4, 14], and also from iterations of the logistic map (1.1), which is not even a diffeomorphism. This extensive experience suggests that the cumulative numerical distortions due to roundoff noise are not arbitrary but constrained by computer shadowing effects that generalize the structural stability of Anosov systems.

Precise results for computer shadowing were first established by Hammel, Yorke, and Grebogi [3, 4]. To be specific, let g_L denote a computer implementation of the general logistic map f_L: $ax_n(1-x_n) = x_{n+1}$, where $0 < a \leqslant 4$, and $0 \leqslant x_n \leqslant 1$. Clearly, g_L and f_L are qualitatively different objects that are not related by a conjugacy transform such as (1.10). Nevertheless, the computer iterations of g_L can be displayed in an array similar to (1.12a) and (1.12b),

$$\begin{array}{ccccccccc} \bar{x}_0 + \bar{\delta}_0 & \to & g_L(\bar{x}'_0) + \bar{\delta}_1 & \to & g_L(\bar{x}'_1) + \bar{\delta}_2 & \to \cdots \to & g_L(\bar{x}'_{j-1}) + \bar{\delta}_j & \to \cdots & (1.17a) \\ \updownarrow & & \updownarrow & & \updownarrow & & \updownarrow & & \\ \bar{x}'_0 & \longrightarrow & \bar{x}'_1 & \longrightarrow & \bar{x}'_2 & \longrightarrow \cdots \longrightarrow & \bar{x}'_j & \longrightarrow \cdots & (1.17b) \end{array}$$

where the $\bar{\delta}_j$'s represent the numerical perturbations introduced by roundoff and truncation. The overbars are notational reminders that all computer numbers have limited precision; e.g., 14 decimal digits on a Cray X-MP. In analogy with (1.14), it is reasonable to assume that all the incremental perturbations in (1.17a) are bounded, i.e.,

$$|g_L(\bar{x}'_{j-1}) - \bar{x}'_j| < \bar{\delta}. \quad (1.18)$$

Consequently all the computer generated iterates of g_L are numerical versions of δ pseudo-trajectories.

The parallel with the Anosov–Bowen theory can now be extended in an obvious way by defining exact trajectories of g_L by means of unperturbed iterations,

$$\bar{x}_0 \to g_L(\bar{x}_0) \to \cdots \to g_L(\bar{x}_j) \to \cdots. \quad (1.19)$$

In analogy with (1.13a), the numerical instability of the g_L-iterations results in a progressive divergence between the exact and approximate computer trajectories. Specifically, if we set

$$|\bar{x}_0 - \bar{x}'_0| = 0, \qquad \text{then} \quad \langle |\bar{x}_j - \bar{x}'_j| \rangle_{j > 50} \sim O(1). \quad (1.20)$$

However, just as in the abstract dynamical theory, the wandering of the computer generated trajectories $\{\bar{x}'_j\}$ is not arbitrary, but constrained by a set of

COMPUTER SHADOWING THEOREMS [3, 4]. *Suppose the logistic map* $g_L: \bar{x}_j \to a\bar{x}_j(1-\bar{x}_j)$ *is iterated on a Cray* X-MP

with 14 digit precision. The step-wise computing noise (1.18) *is then bounded by* $\delta < 3 \times 10^{-14}$. *If the iterations are started at* $\bar{x}_0 = 0.4$, *and the logistic parameter is fixed at* $a = 3.8$, *then there exists an exact trajectory* $\{\bar{y}_j\}$*—generated by* $g_L^j(\bar{y}_0) = \bar{y}_j$, *cf.* (1.19)*—that approximates, or shadows, the computer generated trajectory* $\{\bar{x}'_j\}$ *with a maximum error given by*

$$|\bar{y}_j - \bar{x}'_j| \leqslant 10^{-8}, \qquad 0 \leqslant j \leqslant 10^7. \tag{1.21}$$

Similar results can be obtained for $\bar{x}_0 = 0.4$ *and* $a = 3.6, 3.625, 3.65, 3.75$, *as well as other combinations of* x_0 *and* a.

The method of proof is essentially based on the "inverse" stability criterion (1.7). Starting with the numerical values at the *end* of the computed sequence of iterates, i.e., (1.17b) rewritten in reverse order,

$$\bar{x}'_{10^7} \leftarrow \bar{x}'_{10^7-1} \leftarrow \cdots \leftarrow \bar{x}'_0, \tag{1.22}$$

the existence of a shadowing trajectory $\{\bar{y}_j\}$ is inferred by retrodiction. Specifically let $\bar{y}_{10^7} = \bar{x}'_{10^7}$. Then both of the pre-images $\bar{y}_{10^7-1}$ and $\bar{x}'_{10^7-1}$ will lie in an interval I_{10^7-1}, and similarly the next set of pre-images $\bar{y}_{10^7-2}$ and $\bar{x}'_{10^7-2}$ will lie in an interval I_{10^7-2}. Since these pre-images effectively trace a divergent spray of trajectories backwards, it is plausible that the corresponding intervals satisfy the nesting condition $I_{10^7-1} \supseteq I_{10^7-2}$. In fact the stability criterion (1.7) implies that all of the intervals associated with the reversion of (1.22) are non-expanding, $I_j \supseteq I_{j-1}$. Therefore, if the inclusions $\bar{y}_{10^7-1} \in I_{10^7-1}$ *and* $\bar{x}'_{10^7-1} \in I_{10^7-1}$ yield the initial bound $|\bar{y}_{10^7-1} - \bar{x}'_{10^7-1}| < 10^{-8}$, then it is also plausible that successive pre-image pairs will satisfy (1.21).

Bounding the location of the exact trajectories $\{\bar{y}_j\}$ by means of intervals avoids the need for "error-free" calculations of the individual terms. However, since there is only a heuristic connection between the analytic convergence criterion (1.7) and the behavior of the computer trajectories, the interval inclusions $I_j \supseteq I_{j-1}$ have to be checked by explicit calculations for each choice of a, x_0, and at every step of the reversions, $0 \leqslant j \leqslant N = 10^7$. The variability of the results is illustrated by the fact that the shadowing condition (1.21) is satisfied for $a = 3.75$ and $\bar{x}_0 = 0.4$, but fails if the computer iterations are started at $\bar{x}_0 = 0.3$ [3]. Since the detailed verification of the interval nesting condition $I_j \supseteq I_{j-1}$, involves tedious and time consuming calculations; [illegible] generate an enormous number of trajectories, it is not feasible to amalgamate individual shadowing results such as (1.21) into general theorems concerning the "true" dynamics of computer simulations.

1.6. Shadowing in Čebyšev Mixing Simulations

In the special case of the "fully chaotic" logistic map $4x_n(1 - x_n) = x_{n+1}$, it is possible to show that *all* of the computer generated sequences of iterates are shadowed by exact trajectories. The key idea—following Hammel, Yorke, and Grebogi—is to start at the back end of the computer sequences, and then to construct the shadowing trajectories by step-wise retrodiction. These constructions can be carried out explicitly for the chaotic map (1.1) by adapting a number of results from the theory of Čebyšev mixing transformations:

(1) First, the general Anosov convergence criteria, (1.6) and (1.7), are replaced by a sharper Čebyšev spreading theorem [9, 11, 28]. This ensures that any interval of length $|I| > 0$ is irreversibly dispersed over the entire mixing domain after about $|\log |I||$ iterations. Tracing this interval dispersion pattern backwards generally yields many shadowing trajectories for each computer generated pseudo-trajectory.

(2) None of the logistic maps fit into the framework of the Anosov–Bowen theory because they are not one-to-one functions. However, it is precisely this multiplicity of pre-images that is essential for the construction of shadowing trajectories. The simplest illustration is provided by the iterates of the quadratic Čebyšev polynomial $C_2: x \to x^2 - 2$, $|x| \leqslant 2$, which is conjugate to (1.1):

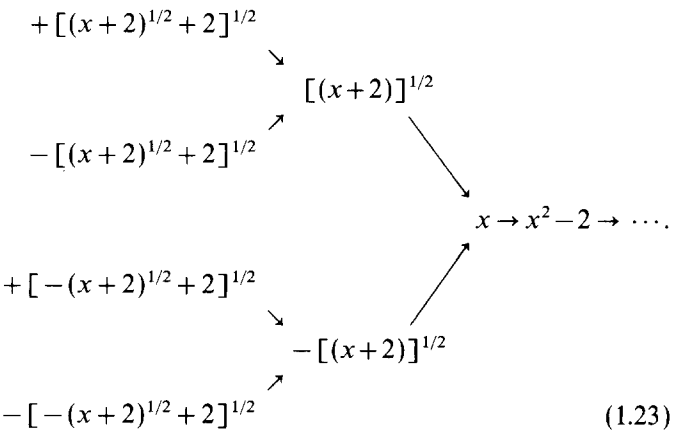

(1.23)

Clearly the element x has two pre-images, or first generation ancestors, and by extension an ancestral tree of g generations contains a total of $2(2^g - 1)$ distinct pre-images for all $x \neq -2$. Since a computer, such as a VAX 3600 operating in double precision, has an ultimate numerical resolution of about one part in 2^{55}, any ancestral tree exceeding 55 [illegible] tion for shadowing is that practically *every* computed value of a Čebyšev iterate can be reached through a pre-image chain in a 55 generation tree rooted at an *arbitrary* initial point! This result complements the preceding Čebyšev spreading estimate, i.e., $|\log_2 2^{-55}| = 55$.

The selection of a pre-image chain leading to a particular ancestral element proceeds in a direction opposite to that of "time's arrow." This arrow is fixed by the convention that forward images correspond to later times. In the case of the

Čebyšev iterates there is a fundamental asymmetry between past and future because none of these mappings is invertible. This is evident from (1.23): the forward mapping $x \to x^2 - 2$ is completely determined by the C_2 algorithm, but the selection of one of the pre-images, $\pm[x+2]^{1/2}$, requires a supplemental rule or some additional information. In this simple but deep sense the past dynamics of a Čebyšev trajectory cannot be recovered by the expedient of "running the film backwards"!

However, pre-images can be selected by retrodiction in order to construct shadowing trajectories. Since the computer generated iterates of a pseudo-trajectory $\{x_j'\}$ are already available, the corresponding shadowing elements are determined simply by choosing the pre-images that most closely match the given x_j' values.

(3) The computer version of the shadowing criterion $|x_j - x_j'| < \varepsilon$ is useful only insofar as the values of the exact iterates x_j are known. In the HYG approach, outlined in Section 1.5, this problem is finessed by means of interval arithmetic. However, in the Čebyšev case more direct methods are available. It is apparent from (1.17a) and (1.19) that the accumulation of errors in the pseudo-trajectories $\{x_j'\}$ is due to the iterative nature of the computations. These errors can be minimized in the Čebyšev simulations by using compact analytical expressions to generate all the requisite pre-images. The numerical evaluation of each iterate is then independent of the results of prior calculations and limited only by the precision of the computers' floating point lattice [29].

(4) Shadowing trajectories for general logistic maps are said to *separate* from pseudo-trajectories at points where the computer trials show that the associated interval nesting conditions are violated [3]. Sharper results may be obtained for the Čebyšev iterations because in these simulations all of the computer generated pseudo-trajectories can be shadowed from end to beginning. Specifically, for a given pseudo-trajectory $\{x_j'\}$ the shadowing sequence of pre-images starts at either a fixed point or terminal cycle and then traces the pseudo-trajectory up to its initial element $\bar{x}_0'$. The shadowing process cannot be continued beyond this point simply because $\bar{x}_0'$ has no pre-images in the set of accessible computer numbers.

The methods used in the construction of shadowing trajectories are explained in detail in Section 2. We begin with the simple case of a Čebyšev computer orbit that terminates in a two-cycle; and progressively extend the techniques until we are able to exhibit a complete shadowing sequence with 33,732,599 elements. Several other applications and extensions are discussed in Section 3. These include the non-uniqueness of shadowing, and the use of shadowing as a measure of complexity in chaotic systems. Finally, in Section 4, we touch on some of the physical implications of the results.

2. CONSTRUCTION OF SHADOWING TRAJECTORIES FOR ČEBYŠEV MIXING SIMULATIONS

2.1. Iterative Properties of Čebyšev Polynomials

All of the iterates of the chaotic logistic function $f_L: x_n \to 4x_n(1-x_n)$, $0 \leqslant x_n \leqslant 1$, are isomorphically mapped onto the iterates of the quadratic Čebyšev polynomial $C_2: x_n \to x_n^2 - 2$, $|x_n| \leqslant 2$, by the linear conjugacy transform

$$C_2 = h \circ f_L \circ h^{-1}, \tag{2.1}$$

where $h = 2(1-2j)$, and j is the identity function. This shift is useful because the iterative properties of the Čebyšev polynomials are well known [7, 9, 30]. Furthermore, both the mathematical results as well as computer trials indicate that the Čebyšev iterations model several of the basic physical characteristics of chaotic systems: these include instability, ergodicity, mixing, fading memory, and the irreversible dispersal of any set of positive measure throughout the domain of the mixing process [8, 10, 11, 28]. As a consequence the shadowing constructions can be developed directly for the Čebyšev mixing simulations. The conjugacy relation (2.1) may be extended further to include piecewise linear "tent" maps which also have the shadowing property [10, 31, 32].

Although the Čebyšev polynomials $C_m(x)$ assume their simplest form in the interval $|x| \leqslant 2$, it is preferable to carry out the machine computations in the interval $1 \leqslant x \leqslant 2$. This avoids some technical difficulties connected with iterations in the vicinity of the machine "zero" [11]. Accordingly we insert $h = 2 - j$ in (2.1); and throughout the rest of this work adopt

$$C_2(x) = 4x^2 - 12x + 10, \qquad 1 \leqslant x \leqslant 2, \tag{2.2}$$

as the standard representation for the quadratic Čebyšev polynomial. The iterates of C_2 can then be obtained from the recursion relation

$$\begin{aligned} &C_2^p(x) = 4[C_2^{p-1}(x)]^2 - 12C_2^{p-1}(x) + 10, \\ &C_2^0(x) \equiv x, \; p \geqslant 1, \; x \in [1, 2]. \end{aligned} \tag{2.3}$$

Due to the shift of the mixing interval the iteration pattern (1.23) becomes more complicated,

$$\begin{array}{l} \tfrac{1}{2}(3 + [x-1]^{1/2}) \\ \qquad\qquad \searrow \\ \qquad\qquad\quad x \to 4x^2 - 12x + 10 \to \cdots, \; x \in [1, 2]. \\ \qquad\qquad \nearrow \\ \tfrac{1}{2}(3 - [x-1]^{1/2}) \end{array} \tag{2.4}$$

However, the iterates are also linked by compact

trigonometric expressions. Specifically, the pth iterate of C_m is given by

$$C_m^p(x) = \tfrac{1}{2}\cos[m^p \cos^{-1}(2x-3)] + \tfrac{3}{2}, \quad p \geqslant 1,\ m \geqslant 0,\ x \in [1,2], \tag{2.5}$$

where $\cos^{-1}$ is evaluated on the principal branch. Similarly, if the set $\{x_{i-1,j}\}_{j=0}^{m-1}$ denotes the m pre-images of the element x_i of C_m, then

$$x_{i-1,j} = \frac{1}{2}\cos\left[\frac{1}{m}\cos^{-1}\{(-1)^j(2x_i-3)\} + \frac{j\pi}{m}\right] + \frac{3}{2}, \quad j = 0, 1, \ldots, m-1,\ m \geqslant 2,\ x_i \in [1,2]. \tag{2.6}$$

In particular, if we represent the values of $x_i \in [1, 2)$ by

$$x_i = \frac{1}{2}\cos\left(\frac{a\pi}{b}\right) + \frac{3}{2}, \qquad \text{where} \quad b \geqslant a > 0, \tag{2.7a}$$

then for C_2, the two pre-images of x_i are

$$x_{i-1,0} = \frac{1}{2}\cos\left(\frac{a\pi}{2b}\right) + \frac{3}{2}$$

and (2.7b)

$$x_{i-1,1} = \frac{1}{2}\cos\left(\frac{2b-a}{2b}\pi\right) + \frac{3}{2}.$$

It is easy to check that these results are equivalent to (2.4).

The four second-generation pre-images of x_i are given by similar expressions:

$$\begin{aligned} x_{i-2,0} &= \frac{1}{2}\cos\left(\frac{a\pi}{4b}\right) + \frac{3}{2}, \\ x_{i-2,1} &= \frac{1}{2}\cos\left(\frac{4b-a}{4b}\pi\right) + \frac{3}{2} \\ x_{i-2,2} &= \frac{1}{2}\cos\left(\frac{2b-a}{4b}\pi\right) + \frac{3}{2}, \\ x_{i-2,3} &= \frac{1}{2}\cos\left(\frac{2b+a}{4b}\pi\right) + \frac{3}{2}. \end{aligned} \tag{2.8}$$

These pre-image relations are the basic building blocks of the Čebyšev shadowing sequence constructions.

The distribution of the numerical values of the Čebyšev iterates $C_m^p(x)$ is governed by the measure

$$P_c(I) = \frac{1}{\pi}\int_I [(2-x)(x-1)]^{-1/2}\,dx, \qquad I \subset [1,2]. \tag{2.9}$$

This means that if the interval I is bounded by two points x_L and x_U, then after a total of N iterations, the inequality

$$1 \leqslant x_L \leqslant C_m^p(x) \leqslant x_U \leqslant 2, \qquad p \leqslant N, \tag{2.10a}$$

will on the average be satisfied $n(I)$ times, where

$$n(I) = \frac{N}{\pi}\{\sin^{-1}(3-2x_L) - \sin^{-1}(3-2x_U)\}. \tag{2.10b}$$

As illustration, if $x_U - x_L \simeq 3\times 10^{-17}$ and the interval is at the edge of the mixing region, e.g., $x_L = 1$, then $n(I)/N \simeq 3.5\times 10^{-9}$. On the other hand, if the interval is at the midpoint, $x_L = 1.5$, then $n(I)/N \simeq 2\times 10^{-17}$. These disparities influence the error bounds of the shadowing sequences.

The Čebyšev spreading theorem gives a quantitative measure of the rate at which the mixing iterations approach the asymptotic statistical distribution (2.10b). If, as in (2.9), I is a subinterval of $[1, 2]$, then its image under iteration, $C_m(I)$, is another interval with measure $P_c(C_m(I))$. N-fold iterations result in an interval with measure $P_c(C_m^N(I))$. The rate of growth of these intervals is then given by the

ČEBYŠEV SPREADING THEOREM [9]. *Suppose I is a subinterval of $[1, 2]$ with positive measure, $P_c(I) > 0$. Let $P_c(C_m^N(I))$ be the measure of the image of this interval after N iterations of the Čebyšev polynomial C_m. Then*

$$P_c(C_m^N(I)) = 1, \qquad \textit{whenever} \quad N > \frac{\log(2/P_c(I))}{\log m}. \tag{2.11}$$

In the special case of C_2, and an interval of length $|I| = x_U - x_L \simeq 3\times 10^{-17} \simeq 2^{-55}$, located at $x_L = 1.5$, Eq. (2.11) indicates that 57 iterations suffice to disperse I over the entire mixing range $[1, 2]$. Evidently the spreading theorem strengthens the analogies between mathematical and physical mixing processes.

The spreading of intervals is also directly related to the instability of the Čebyšev iterations. Let $\{C_m^p(x_0)\}$ and $\{C_m^p(y_0)\}$ denote two sequences of iterates whose initial points are included in an arbitrarily small interval, i.e., x_0, $y_0 \in I$, and $P_c(I) > 0$. Mixing implies that for almost all choices of x_0 and y_0, and $m \geqslant 2$, both $\{C_m^p(x_0)\}$ and $\{C_m^p(y_0)\}$ behave as independent identically distributed random variables with a common distribution function [33]. It can then be shown that the average asymptotic distance between iterates is of the order of the diameter of the mixing region [8, 25]:

$$\langle |C_m^p(x_0) - C_m^p(y_0)| \rangle_{p \gg 1} \sim O(1), \qquad m \geqslant 2. \tag{2.12}$$

Comparing (2.11) and (2.12) with the Liapunov criteria (1.2a) and (1.2b), it is evident that the Čebyšev iterates are dynamically unstable. The connection between these results and the Poincaré recurrence theorem is discussed in detail in Ref. [28].

2.2. Shadowing Trajectories for an Orbit with a Two-Cycle

It is convenient to begin the construction of the Čebyšev shadowing sequences with one of the simplest orbits of C_2: namely, the set of all iterates that merge into a terminal two-cycle. The two elements of this two-cycle are the solutions of the iterative equation

$$C_2^2(x) = x, \qquad x \in [1, 2]. \tag{2.13a}$$

[illegible] are

$$x_{1U} = \frac{1}{2}\cos\left(\frac{2\pi}{5}\right) + \frac{3}{2} \cong 1.65450849718747373 \equiv \bar{x}_{1U} \tag{2.13b}$$

and

$$x_{1D} = \frac{1}{2}\cos\left(\frac{4\pi}{5}\right) + \frac{3}{2} \cong 1.09549150281252627 \equiv \bar{x}_{1D} \tag{2.13c}$$

where evidently

$$C_2(x_{1U}) = x_{1D}, \qquad C_2(x_{1D}) = x_{1U}. \tag{2.13d}$$

Each element of the two-cycle has two pre-images: one pre-image is simply the other element of the cycle, while the second pre-image lies off the cycle and feeds into it. Each of these "off cycle" pre-images is in turn the origin of an infinite ancestor tree—such as (1.23) or (2.4)—with a doubling of the number of pre-images at each additional generation away from the cycle. Figure 1 shows the iterate structure around the two-cycle in pictorial and analytic form.

Now let us check to what extent this structure can be reproduced on a computer. The most elementary tests consist of substituting the 18-digit number $\bar{x}_{1U}$ into the expression

$$\bar{C}_2(\bar{x}) \equiv 4\bar{x}^2 - 12\bar{x} + 10 \tag{2.14}$$

and verifying that

and, also,

$$\bar{C}_2^2(\bar{x}_{1U}) = \bar{x}_{1U}, \tag{2.15b}$$

where

$$\bar{C}_2^2(\bar{x}) \equiv 4[\bar{C}_2(\bar{x})]^2 - 12\bar{C}_2(\bar{x}) + 10. \tag{2.16}$$

The crucial distinction between (2.2), (2.3), and (2.14), (2.16) is that $\bar{C}_2(\bar{x})$ *now denotes the computer implementation of the Čebyšev algorithms.* In the present calculations

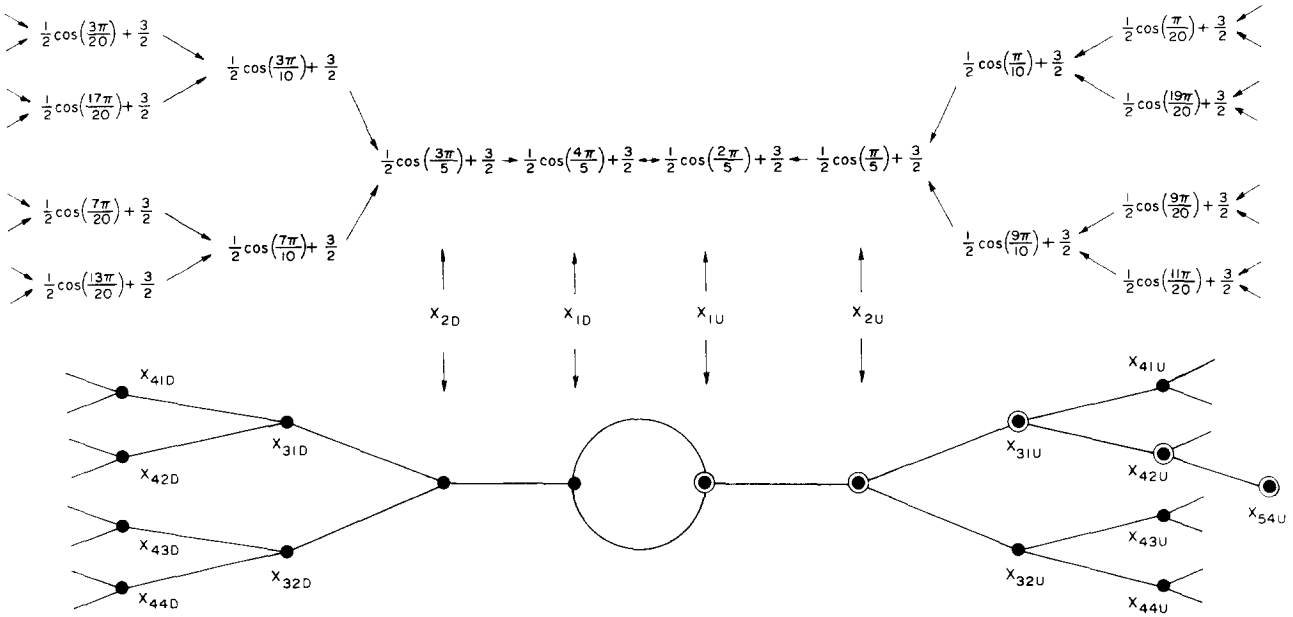

FIG. 1. Exact two-cycle orbit of the quadratic Čebyšev polynomial. The diagram shows the trigonometric representations of the orbit elements surrounding the terminal loop. Some of these elements are also listed in column one of Table I. Corresponding points in Fig. 1 and Fig. 2, are labeled by the symbols, x_{1U}, x_{2U}, etc.

this means double precision floating point arithmetic on a VAX 3600, where all algorithms are programmed in FORTRAN 77 for a DEC Ada compiler. $C_2(x)$ and $\bar{C}_2(\bar{x})$ are related in precisely the same way as the logistic maps f_L and g_L in Section 1.5.

The numerical identities (2.15a) and (2.15b) are simple but not trivial: They happen to be satisfied for the $\bar{C}_2$ two-cycle, but already fail for one of the $\bar{C}_2$ three-cycles, i.e., the solutions of $\bar{C}_2^3(\bar{x}) = \bar{x}$. This lack of periodicity of the machine iterates of $\bar{C}_2(\bar{x})$ is displayed in the following array:

$$
\begin{aligned}
x_1 &\equiv \frac{1}{2}\cos\left(\frac{2\pi}{7}\right)+\frac{3}{2} \simeq 1.811\,744\,900\,929\,366\,77 \equiv \bar{x}_1 \\
C_2(x_1) &= \frac{1}{2}\cos\left(\frac{4\pi}{7}\right)+\frac{3}{2} \simeq 1.388\,739\,533\,021\,842\,80 \\
&\neq 1.3\cdots4283 = \bar{C}_2(\bar{x}_1) \\
C_2^2(x_1) &= \frac{1}{2}\cos\left(\frac{8\pi}{7}\right)+\frac{3}{2} \simeq 1.049\,515\,566\,048\,790\,43 \\
&\neq 1.0\cdots9048 = \bar{C}_2^2(\bar{x}_1) \\
C_2^3(x_1) &= \frac{1}{2}\cos\left(\frac{2\pi}{7}\right)+\frac{3}{2} \simeq 1.8\cdots366\,77 \neq 1.8\cdots36646 = \bar{C}_2^3(\bar{x}_1) \\
&\vdots \qquad\qquad \vdots \qquad\qquad \vdots \qquad\qquad \vdots \\
C_2^6(x_1) &= \frac{1}{2}\cos\left(\frac{2\pi}{7}\right)+\frac{3}{2} \simeq 1.8\cdots366\,77 \neq 1.8\cdots36424 = \bar{C}_2^6(\bar{x}_1).
\end{aligned}
\tag{2.17}
$$

The underlined digits exhibit the progressive divergence between the iterates of C_2 and $\bar{C}_2$.

Suppose now we return to the two-cycle and check further to see how much more of the pre-image structure displayed in Fig. 1 can be simulated by the computer iterations. A simple starting point is the two-cycle element x_{1D}: nominally it has two pre-images, x_{1U} and x_{2D}, given by

$$x_{1U} = \frac{1}{2}\cos\left(\frac{2\pi}{5}\right)+\frac{3}{2} \simeq 1.654\,508\,497\,187\,473\,73 \equiv \bar{x}_{1U} \tag{2.18a}$$

$$\downarrow$$

$$x_{1D} = \frac{1}{2}\cos\left(\frac{4\pi}{5}\right)+\frac{3}{2} \simeq 1.095\,491\,502\,812\,526\,27 \equiv \bar{x}_{1D} \tag{2.18b}$$

$$\uparrow$$

$$x_{2D} = \frac{1}{2}\cos\left(\frac{3\pi}{5}\right)+\frac{3}{2} \simeq 1.345\,491\,502\,812\,526\,27 \equiv \bar{x}_{2D}. \tag{2.18c}$$

On a computer we should therefore be able to verify the numerical iterations

$$\bar{C}_2(\bar{x}_{1U}) = \bar{x}_{1D} \tag{2.19a}$$

and

$$\bar{C}_2(\bar{x}_{2D}) = \bar{x}_{1D}. \tag{2.19b}$$

These relations are indeed satisfied; but the instability of the Čebyšev iterations raises the suspicion that there may be additional parasitic pre-images. In order to check on this possibility we construct numerical "fans," or intervals, about each nominal pre-image value. For the pre-image x_{1U} in (2.18a), this fan is given by the set of contiguous numbers

$$\mathrm{Fan}(x_{1U}) \equiv \{1.654\,508\,497\,187\,473\,73 \pm n\varepsilon\}_{n=0}^{32000} \tag{2.20a}$$

and similarly for x_{2D} in (2.18c),

$$\mathrm{Fan}(x_{2D}) \equiv \{1.345\,491\,502\,812\,526\,27 \pm n\varepsilon\}_{n=0}^{32000}. \tag{2.20b}$$

The ε corresponds to the machine's limit of numerical resolution, $\varepsilon = 2^{-55} \sim 2.78 \times 10^{-17}$; and therefore each fan has a total width of $\sim 1.8 \times 10^{-12}$.

The search for parasitic pre-images then consists simply of computing all of the 128,000 forward images of the fan sets, $\bar{C}_2[\mathrm{Fan}(x_{1U})]$ and $\bar{C}_2[\mathrm{Fan}(x_{2D})]$, and checking whether any of the results yields x_{1D}. For the first fan we find four additional pre-images,

$$\left.\begin{aligned} C_2(1.654\cdots7359) \\ C_2(1.654\cdots7370) \\ C_2(x_{1U} = 1.654\cdots7373) \\ C_2(1.654\cdots7375) \\ C_2(1.654\cdots7378) \end{aligned}\right\} = \bar{x}_{1D} \tag{2.21a}$$

and for the second, six additional pre-images,

$$\left.\begin{aligned} C_2(1.345\cdots2611) \\ C_2(1.345\cdots2619) \\ C_2(1.345\cdots2622) \\ C_2(1.345\cdots2625) \\ C_2(x_{2D} = 1.345\cdots2627) \\ C_2(1.345\cdots2630) \\ C_2(1.345\cdots2636) \end{aligned}\right\} = \bar{x}_{1D}. \tag{2.21b}$$

These results show that even on the first pre-image step away from the two-cycle—i.e., $x_{2D} \to x_{1D}$ in Fig. 1—there are significant differences between the iterative structure of C_2 and its computer implementation $\bar{C}_2$. By similar methods it is possible to find six ancestors of $\bar{x}_{2D}$: Two of these correspond to the analytic pre-images x_{31D} and x_{32D} shown in Fig. 1, and the other four are parasitic pre-images clustered about x_{31D} and x_{32D}.

A distinctive new feature appears in the "ancestor hunt" for the next generation of pre-images, i.e., the elements

$x_{41D} - x_{44D}$ in Fig. 1. Suppose that as usual the analytic values

$$x_{41D} = \frac{1}{2}\cos\left(\frac{3\pi}{20}\right) + \frac{3}{2} \simeq 1.945\,503\,262\,094\,183\,92 \equiv \bar{x}_{41D} \tag{2.22a}$$

$$x_{42D} = \frac{1}{2}\cos\left(\frac{17\pi}{20}\right) + \frac{3}{2} \simeq 1.054\,496\,737\,905\,816\,08 \equiv \bar{x}_{42D} \tag{2.22b}$$

$$x_{43D} = \frac{1}{2}\cos\left(\frac{7\pi}{20}\right) + \frac{3}{2} \simeq 1.726\,995\,249\,869\,773\,40 \equiv \bar{x}_{43D} \tag{2.22c}$$

$$x_{44D} = \frac{1}{2}\cos\left(\frac{13\pi}{20}\right) + \frac{3}{2} \simeq 1.273\,004\,750\,130\,226\,60 \equiv \bar{x}_{44D} \tag{2.22d}$$

are taken as the center points for the pre-image fan constructions:

$$\begin{aligned} \text{Fan}(x_{41D}) &= \{x_{41D} \pm n\varepsilon\}_{n=0}^{32000}, \\ \text{Fan}(x_{42D}) &= \{x_{42D} \pm n\varepsilon\}_{n=0}^{32000} \\ \text{Fan}(x_{43D}) &= \{x_{43D} \pm n\varepsilon\}_{n=0}^{32000}, \\ \text{Fan}(x_{44D}) &= \{x_{44D} \pm n\varepsilon\}_{n=0}^{32000}. \end{aligned} \tag{2.23}$$

The computer trials then show that *none of the* 256,000 *forward images of any of the numbers in the four fan sets in* (2.23) *coincide with either* $\bar{x}_{31D}$ or $\bar{x}_{32D}$. Specifically,

$$\bar{C}_2[\text{Fan}(x_{41D})] \neq \bar{x}_{31D} \neq \bar{C}_2[\text{Fan}(x_{42D})], \tag{2.24a}$$

where

$$\bar{x}_{31D} \equiv 1.793\,892\,626\,146\,236\,57 \simeq \frac{1}{2}\cos\left(\frac{3\pi}{10}\right) + \frac{3}{2} = x_{31D}, \tag{2.24b}$$

and

$$\bar{C}_2[\text{Fan}(x_{43D})] \neq x_{32D} \neq \bar{C}_2[\text{Fan}(x_{44D})], \tag{2.25a}$$

where

$$\bar{x}_{32D} \equiv 1.206\,107\,373\,853\,763\,43 \simeq \frac{1}{2}\cos\left(\frac{7\pi}{10}\right) + \frac{3}{2} = x_{32D}. \tag{2.25b}$$

In this sense it is possible to verify that there are computer numbers such as $\bar{x}_{31D}$ and $\bar{x}_{32D}$ that have no pre-images whatsoever with respect to the machine-implemented $\bar{C}_2$ algorithm—informally speaking, they are "*orphan points.*" The finite length of all the iterative sequences on a computer is an obvious consequence of non-existence relations such as (2.24a) and (2.25a).

If we now take the exact C_2 iteration pattern in Fig. 1 as a template, it is possible to use the pre-image fan technique to map out the entire two-cycle orbit of the machine algorithm $\bar{C}_2$. The results are displayed in Fig. 2. Clearly, the two structures shown on Figs. 1 and 2 have only a superficial resemblance. The open circles in Fig. 2 denote orphan points: they cluster about *all* of the filled circles that denote points with pre-images. However, to avoid confusion in Fig. 2, we show the full complement of orphan points only for x_{1D}, x_{2D}, x_{1U}, and x_{19U}. The most striking characteristic of the computer two-cycle is that its pre-images capture so little of the exact analytic orbit: there are only 100 interior or non-orphan points in Fig. 2; and the entire pattern is bounded by 702 orphan points. The longest run of iterates shared by C_2 and $\bar{C}_2$ is the 20 element sequence marked by the double circles in Figs. 1 and 2. Table I shows

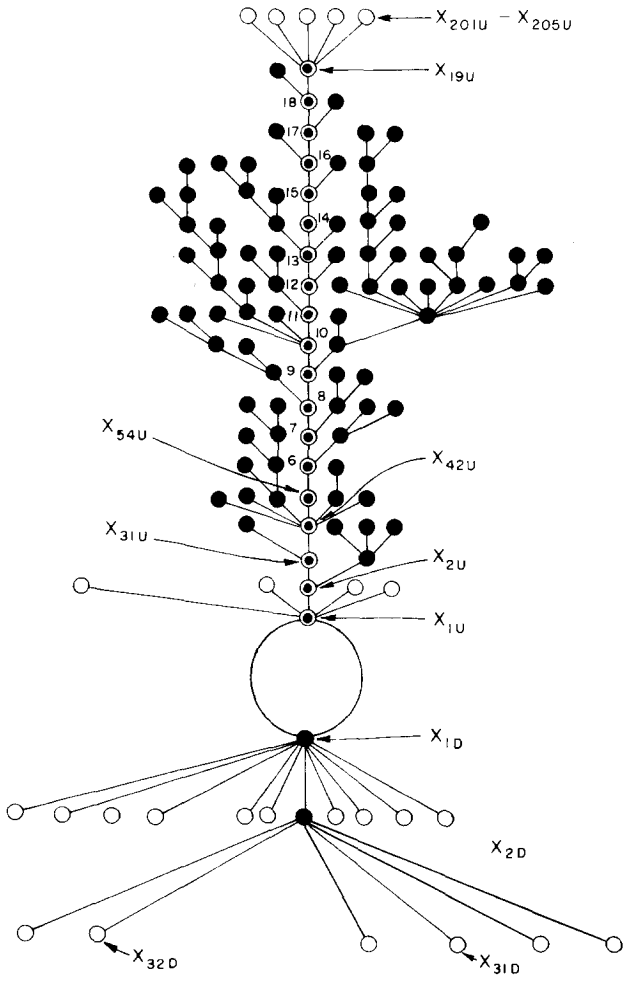

FIG. 2. Computer generated two-cycle orbit of the quadratic Čebyšev polynomial. The open circles indicate orphan points; the filled circles denote interior points: The double circles in Fig. 1 and Fig. 2 mark the shadowed trajectory shown in Table I. The computer orbit is conspicuously asymmetric.

TABLE I

Shadowing on the Principal Branch of the $\bar{C}_2(\bar{x})$ Two-Cycle

Label of point on Fig. 2	$C_2(x)$	$\bar{C}_2(\bar{x})$	$\delta \times 10^{17}$
x_{19U}	$\frac{1}{2}\cos\left(\frac{234139\pi}{655360}\right)+\frac{3}{2}\approx 1.71676508377677536$	$1.71\cdots 539$	3
18	$\frac{1}{2}\cos\left(\frac{234139\pi}{327680}\right)+\frac{3}{2}\approx 1.18794840617900976$	$1.18\cdots 976$	0
17	$\frac{1}{2}\cos\left(\frac{93541\pi}{163840}\right)+\frac{3}{2}\approx 1.38950478882488110$	$1.38\cdots 104$	6
16	$\frac{1}{2}\cos\left(\frac{70299\pi}{81920}\right)+\frac{3}{2}\approx 1.04883676677053647$	$1.04\cdots 650$	3
15	$\frac{1}{2}\cos\left(\frac{11621\pi}{40960}\right)+\frac{3}{2}\approx 1.81419305207225320$	$1.81\cdots 312$	8
14	$\frac{1}{2}\cos\left(\frac{11621\pi}{20480}\right)+\frac{3}{2}\approx 1.39486909588191046$	$1.39\cdots 033$	13
13	$\frac{1}{2}\cos\left(\frac{8859\pi}{10240}\right)+\frac{3}{2}\approx 1.04421002800274776$	$1.04\cdots 776$	0
12	$\frac{1}{2}\cos\left(\frac{1381\pi}{5120}\right)+\frac{3}{2}\approx 1.83097799429302396$	$1.83\cdots 399$	3
11	$\frac{1}{2}\cos\left(\frac{1381\pi}{2560}\right)+\frac{3}{2}\approx 1.43818573082493203$	$1.43\cdots 195$	8
10	$\frac{1}{2}\cos\left(\frac{1179\pi}{1280}\right)+\frac{3}{2}\approx 1.01528401549459105$	$1.01\cdots 102$	3
9	$\frac{1}{2}\cos\left(\frac{101\pi}{640}\right)+\frac{3}{2}\approx 1.93979834254019146$	$1.93\cdots 146$	0
8	$\frac{1}{2}\cos\left(\frac{101\pi}{320}\right)+\frac{3}{2}\approx 1.77369032840439828$	$1.77\cdots 833$	5
7	$\frac{1}{2}\cos\left(\frac{101\pi}{160}\right)+\frac{3}{2}\approx 1.29962558344842952$	$1.29\cdots 960$	8
6	$\frac{1}{2}\cos\left(\frac{59\pi}{80}\right)+\frac{3}{2}\approx 1.16059962723352914$	$1.16\cdots 905$	9
x_{54U}	$\frac{1}{2}\cos\left(\frac{21\pi}{40}\right)+\frac{3}{2}\approx 1.46077045213607754$	$1.46\cdots 759$	5
x_{42U}	$\frac{1}{2}\cos\left(\frac{19\pi}{20}\right)+\frac{3}{2}\approx 1.00615582970243114$	$1.00\cdots 111$	3
x_{31U}	$\frac{1}{2}\cos\left(\frac{\pi}{10}\right)+\frac{3}{2}\approx 1.97552825814757679$	$1.97\cdots 682$	3
x_{2U}	$\frac{1}{2}\cos\left(\frac{\pi}{5}\right)+\frac{3}{2}\approx 1.90450849718747373$	$1.90\cdots 373$	0
x_{1U}	$\frac{1}{2}\cos\left(\frac{2\pi}{5}\right)+\frac{3}{2}\approx 1.65450849718747373$	$1.65\cdots 373$	0

that the numerical values of the computer iterates differ from the exact trajectory by at most 1.3×10^{-16}, and therefore this qualifies as our first example of a "shadowing trajectory"!

A numerical inventory of all of the 802 elements of the [illegible] has a "wild" or arbitrary value. The maximum difference between corresponding sets of elements of the approximate ($\bar{C}_2$) and exact (C_2) two-cycle orbits is less than 10^{-15}. In this respect the computer two-cycle orbit in Fig. 2 is precisely "shadowed" by a fragment of the exact orbit in Fig. 1. However, this numerical correspondence does *not* imply that the approximate iteration pattern in Fig. 2 is a template for the exact orbit in Fig. 1. In fact, the gap between numerical and structural information is even more conspicuous for other "short cycle" Čebyšev orbits.

Let $N(m, l)$ denote the number of cycles of length l of the mth order Čebyšev polynomial C_m. Then evidently $N(m, 1) = m$, since the mth degree Čebyšev polynomial has m fixed points, or one-cycles. The general result is [34]

$$N(m, l) = \frac{1}{l} \sum_{d} \mu(d)\, m^{l/d}, \qquad m \geqslant 2, \tag{2.26}$$

where $\mu(d)$ is the Möbius function, and d is the set of divisors of l. (For example, if $l = 6$, $d \to 1, 2, 3, 6$; etc.). Table II lists some numerical values of $N(m, l)$. The results of a computer search for some of these short cycles are summarized in Table III(a). As usual, $\bar{C}_m$ represents the computer implementation of the Čebyšev recursion algorithms. Some of the entries in the column under $\bar{C}_2$ in Table III(a) are already familiar: For $l = 1$, the entry "2" corresponds to the two fixed points at 2 and 1.25; for $l = 2$, the entry "1" denotes the computer two-cycle found earlier in (2.15a) and (2.15b); for $l = 3$, the entry "1" corresponds to the three-cycle

$$\frac{1}{2}\cos\left(\frac{2\pi}{9}\right) + \frac{3}{2} \to \frac{1}{2}\cos\left(\frac{4\pi}{9}\right) + \frac{3}{2} \to \frac{1}{2}\cos\left(\frac{8\pi}{9}\right) + \frac{3}{2} \tag{2.27}$$

which *can* be simulated by the computer, whereas we have already seen in (2.17) that the other three-cycle *cannot* be simulated. The overall trend of the results collected in Table III(a) indicates that the computer's floating point lattice is not suited to approximating the iterative behavior of the short cycle Čebyšev orbits. This mismatch is also evident in the computer generated orbit statistics summarized in [illegible] Table III(b) show that only negligible fragments of the exact C_2–C_5 short cycle orbits are reproduced by the computer simulations.

The large value of the ratio ⟨(orphan points)/(interior points)⟩ ~ 7, shows that on the average the tendency to have very few or no pre-images (e.g., (2.24a) and (2.25a)) predominates over the occurrence of many pre-images (e.g., (2.21a) and (2,21b)). Extensive computer explorations of the orbits of Čebyšev polynomial recursions confirm that this is a generally valid result [11]. As a consequence, if numbers are selected with uniform probability from the set of 2^{55} computer numbers available in the interval [1, 2], then 87% of the chosen numbers will be orphan or initial points of the Čebyšev mixing simulations. All of the interior elements that usually appear in pseudo-random number generators, cryptographic applications, or in the simulation of chaotic systems comprise only a small fraction of the total pool of accessible numbers.

TABLE II

Number of Cycles of Length l of the Čebyšev Polynomial C_m: $N(m, l)$, cf. (2.26)

Order of polynomial m / Cycle length l	2	3	4	5	6
1	2	3	4	5	6
2	1	3	6	10	15
3	2	8	18	40	70
4	3	18	60	150	315
5	6	48	198	624	1554
6	9	116	670	2580	7735

TABLE III(a)

Cycles of Length l Found in a Search by a VAX 3600 in Double Precision

	C_2	$\bar{C}_2$	C_3	$\bar{C}_3$	C_4	$\bar{C}_4$	C_5	$\bar{C}_5$
Cycle length l	$N(2,l)$	Found by VAX	$N(3,l)$	Found by VAX	$N(4,l)$	Found by VAX	$N(5,l)$	Found by VAX
1	2	2	3	3	4	3	5	5
2	1	1	3	2	6	0	10	1
3	2	1	8	1	18	0	40	0
4	3	0	18	0	60	0	150	1
5	6	0	48	0	198	1	624	0
6	9	0	116	0	670	0	2580	—

TABLE III(b)

Computer Generated Čebyšev Orbits Terminating in Short Cycles

Orbit	Total no. of elements in orbit	Number of orphan points	Number of interior points	Orphan points / Interior points	Length of longest trajectory
C_2: 2-cycle	802	702	100	7	20
C_2: 3-cycle	64	56	8	7	4
C_3: 2-cycle	21	18	3	6	3
C_3: 2-cycle	16	14	2	7	2
C_3: 3-cycle	267	234	33	7.09	11
C_4: 5-cycle	164	140	24	5.83	7
C_5: 2-cycle	1890	1651	239	6.91	30
C_5: 4-cycle	52	45	7	6.43	3

2.3. Shadowing Trajectories Emerging from a Fixed Point

The first six generations of pre-images of the $C_2(x)$ fixed point at $x = 2$ are shown in Fig. 3. In particular, as indicated in (2.4), the point 1 has the unique pre-image $\frac{3}{2}$. However, because of the peaking of the Čebyšev measure (2.10b) at both ends of the mixing interval [1, 2], the computer algorithm $\bar{C}_2$ has a strikingly different pre-image pattern. The fan technique introduced in (2.20a) and (2.20b) can be used to verify that the end point 1 has more than 10^8 computer pre-images in the interval [1.499 999 992 320 117 32, 1.500 000 007 679 882 67]. About 98% of these parasitic pre-images have short ancestral lines not exceeding 60 generations. One of the longest of these "short stubs" is shown in Table IV: the corresponding pre-image sequence in Fig. 3 is marked by an asterisk. The close correspondence between the exact (C_2) and computer generated values ($\bar{C}_2$) shows that this is another shadowing pair analogous to

[redacted]

shadowing length is limited to 57 steps because $\bar{C}_2(\bar{x}) \sim 1.947\cdots897$ is one of the four orphan points that is the source of the computer trajectory.

The dagger in Fig. 3 marks the beginning of another shadowing sequence that follows a computer generated trajectory for 1, 331, 038 iterations back to its inception at the orphan point 1.014 214 634 895 324 71. Such long shadowing runs require an extension of the pre-image construction methods. It is obvious from (2.7a) and (2.7b) that if a particular element is represented by $\cos(a\pi/b)$, then its eightieth generation ancestors will include pre-images proportional to $\cos(A\pi/B)$, where A and B are both large numbers of the order of 2^{80}. It is just barely feasible to evaluate such trigonometric expressions with multiple precision routines without encountering arithmetic overflow. But this is certainly not possible in pre-image searches extending over hundreds of thousands of generations.

In the Appendix we outline a simple procedure that avoids computer overflow. In essence: (1) the ratio A/B is simplified by removing powers of ten that occur as common factors; and (2) only the most significant figures in the ratio are retained for *quadruple* precision computations. It can then be shown that these approximations introduce errors

[redacted]

Čebyšev iterations. By combining these approximations with the pre-image representation (2.27b), it becomes feasible to construct shadowing sequences that are not overwhelmed by computer roundoff even after millions of terms.

If, for clarity, we distinguish Čebyšev elements constructed by the methods of the Appendix by the notation $\tilde{C}_2$, then the entire shadowing procedure can be summarized in terms of the following array:

(i) Exact Čebyšev iterations

$$x_0 \to C_2(x_0) \to C_2^2(x_0) \to \cdots \to x_N. \tag{2.28}$$

(ii) Čebyšev iterations generated by computer recursions

$$\bar{x}_0 \to \bar{C}_2(\bar{x}_0) \to \bar{C}_2^2(\bar{x}_0) \to \cdots \to \bar{x}'_N. \tag{2.29}$$

(iii) Čebyšev pre-images computed by analytic and approximate means: each pre-image is selected by retrodiction to achieve the closest possible match to the iteration sequence in (2.29)

$$\bar{y}_0 \leftarrow \tilde{C}_2(\bar{y}_0) \leftarrow \cdots \leftarrow \tilde{C}_2(\bar{y}_{N-2}) \leftarrow \tilde{C}_2(\bar{y}_{N-1}) = \bar{y}_N \equiv \bar{x}'_N. \tag{2.30}$$

Clearly these sequences are the analogues of the basic shadowing triad of the Anosov–Bowen theory (Section 1.4): The analytic Čebyšev iterates $C_2^n(x_0)$ correspond to the exact Anosov trajectories $\{x_j\}$; the computer iterates $\bar{C}_2^n(\bar{x}_0)$ mimic the perturbed δ pseudo-trajectories $\{x'_j\}$; and the pre-images $\tilde{C}_2(\bar{y}_j)$ are surrogates for the exact shadowing sequences $\{y_j\}$.

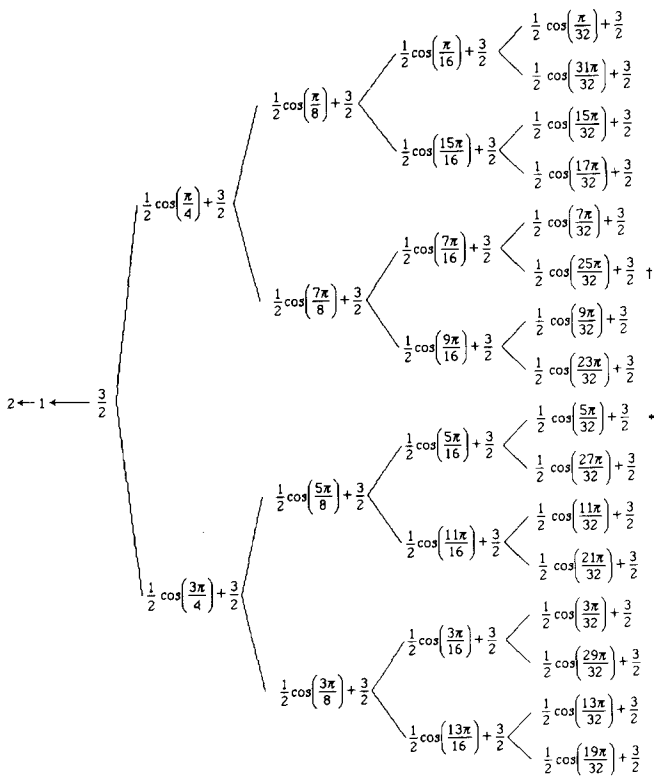

FIG. 3. Pre-images of the fixed point "2." The asterisk indicate the trajectory of the 57-element shadowing sequence in Table IV. The dagger marks the beginning of another shadowing sequence with 1,331,038 iterates.

TABLE IV

Trajectory Emerging from a Fixed Point

Number of generations from fixed point	$C_2(x)$	$\bar{C}_2(\bar{x})$	$\delta \times 10^{17}$
57	$\frac{1}{2}\cos\left(\frac{10561281022968443\pi}{72057594037927936}\right)+\frac{3}{2}\approx 1.94792531701016894$	$1.947\cdots 897$	3
56	$\frac{1}{2}\cos\left(\frac{10561281022968443\pi}{36028797018963968}\right)+\frac{3}{2}\approx 1.80254835847464135$	$1.802\cdots 134$	1
55	$\frac{1}{2}\cos\left(\frac{10561281022968443\pi}{18014398509481984}\right)+\frac{3}{2}\approx 1.36614203686280034$	$1.366\cdots 034$	0
54	$\frac{1}{2}\cos\left(\frac{7453117486513541\pi}{9007199254740992}\right)+\frac{3}{2}\approx 1.07167181718095961$	$1.071\cdots 961$	0
53	$\frac{1}{2}\cos\left(\frac{1554081768227451\pi}{4503599627370496}\right)+\frac{3}{2}\approx 1.73386012878824514$	$1.733\cdots 514$	0
52	$\frac{1}{2}\cos\left(\frac{1554081768227451\pi}{2251799813685248}\right)+\frac{3}{2}\approx 1.21876223934741841$	$1.218\cdots 845$	4
51	$\frac{1}{2}\cos\left(\frac{697718045457797\pi}{1125899906842624}\right)+\frac{3}{2}\approx 1.31637871206751507$	$1.316\cdots 500$	7
50	$\frac{1}{2}\cos\left(\frac{428181861384827\pi}{562949953421312}\right)+\frac{3}{2}\approx 1.13486710952793814$	$1.134\cdots 812$	2
49	$\frac{1}{2}\cos\left(\frac{134768092036485\pi}{281474976710656}\right)+\frac{3}{2}\approx 1.53328811081793090$	$1.533\cdots 082$	8
8	$\frac{1}{2}\cos\left(\frac{123\pi}{128}\right)+\frac{3}{2}\approx 1.00376023270064500$	$1.003\cdots 496$	4
7	$\frac{1}{2}\cos\left(\frac{5\pi}{64}\right)+\frac{3}{2}\approx 1.98501562659727200$	$1.985\cdots 204$	4
6	$\frac{1}{2}\cos\left(\frac{5\pi}{32}\right)+\frac{3}{2}\approx 1.94096063217417751$	$1.940\cdots 769$	18
5	$\frac{1}{2}\cos\left(\frac{5\pi}{16}\right)+\frac{3}{2}\approx 1.77778511650980111$	$1.777\cdots 175$	64
4	$\frac{1}{2}\cos\left(\frac{5\pi}{8}\right)+\frac{3}{2}\approx 1.30865828381745511$	$1.308\cdots 652$	141
3	$\frac{1}{2}\cos\left(\frac{3\pi}{4}\right)+\frac{3}{2}\approx 1.14644660940672624$	$1.146\cdots 405$	219
2	$\frac{1}{2}\cos\left(\frac{\pi}{2}\right)+\frac{3}{2}\approx 1.50000000000000000$	$1.500\cdots 622$	622
1	$\frac{1}{2}\cos(\pi)+\frac{3}{2}\approx 1.00000000000000000$	$1.000\cdots 000$	0
0	$\frac{1}{2}\cos(0)+\frac{3}{2}\approx 2.00000000000000000$	$2.000\cdots 000$	0

Table V exhibits the trend in shadowing errors that results when the long ($\sim 1.33 \times 10^6$) $\bar{C}_2$ iteration trajectory is tracked by a $\tilde{C}_2$ pre-image sequence. The new feature in this situation is the large error jump ($\delta \sim 4 \times 10^{-9}$) that occurs at the second pre-image generation. As indicated in the table, this shadowing error can be reduced by a factor of 10^7 through appropriate choices of pre-images in the next 26 generations. This rapid gain in precision is basically due to the fact that the $\tilde{C}_2$ pre-image sequences satisfy a reversed version of the Čebyšev spreading theorem (2.11). If, for example, the particular element $\bar{C}_2 \to 1.295\cdots$, in the 29th generation in Table V, is chosen as a "target" value, then (2.11) implies that it is likely that one of the 2^{29}, 29-generation pre-image sequences emerging from the fixed point 2 will "hit" close to this target. Indeed, Table V shows that the corresponding shadowing error is only 6×10^{-17}.

However, the confluence of the iteration ($\bar{C}_2$) and shadowing ($\tilde{C}_2$) trajectories displayed in Table V is only part of a more complicated pattern. Table VI shows that large shadowing errors of the order of 10^{-12} tend to recur in spikes at iteration intervals of roughly 10^5 steps. In every case, the $\bar{C}_2$ and $\tilde{C}_2$ elements agree exactly, in double precision, when they approach 1, but the shadowing error jumps

TABLE V

Confluence of a Long Shadowing Trajectory Emerging from a Fixed Point

Number of generations from fixed point	$\bar{C}_2$	$\tilde{C}_2$	$\delta \times 10^{17}$
29	1.29543250839522672	1.29543250839522678	6
28	1.16739143448587579	1.16739143448587585	6
27	1.44251383141345380	1.44251383141345368	12
26	1.01321863831504322	1.01321863831504330	8
25	1.94782437633544281	1.94782437633544256	25
24	1.80218668816091321	1.80218668816091229	92
23	1.36526717800664388	1.36526717800664182	206
22	1.07261173328917359	1.07261173328917578	219
21	1.73064292208833792	1.73064292208833045	747
20	1.21278463003778847	1.21278463003777470	1.377
19	1.32997067497012011	1.32997067497015187	3.176
18	1.11563988548046611	1.11563988548042298	4,313
17	1.59093079053387676	1.59093079053400940	13,264
16	1.03307363466846303	1.03307363466855959	9,656
15	1.87208092256687975	1.87208092256651906	36,069
14	1.55377685175288138	1.55377685175180782	107,356
13	1.01156779913780559	1.01156779913734365	46,194
12	1.95426405935634806	1.95426405935815306	180,500
11	1.82542334249163085	1.82542334249819047	655,962
10	1.42360140735370111	1.42360140737077828	1,707,717
9	1.02334697983334033	1.02334697982290310	1,043,723
8	1.90879240653599225	1.90879240657579186	3,979,961
7	1.66844492656595178	1.66844492669611003	13,015,825
6	1.11349477314323564	1.11349477331863153	17,539,589
5	1.59754516155039550	1.59754516100806412	54,233,138
4	1.03806023416757109	1.03806023374435663	42,321,446
3	1.85355338902927702	1.85355339059327376	156,399,674
2	1.49999999557634922	1.50000000000000000	442,365,078
1	1.00000000000000000	1.00000000000000000	0
0	2.00000000000000000	2.00000000000000000	0

TABLE VI

Location of Large Jumps in the Shadowing Distance: 1.33×10^6 Iterations Terminating at 2

Number of generations from fixed point	$\bar{C}_2$	$\delta = \lvert\bar{C}_2 - \tilde{C}_2\rvert$
1,298,510	1.50000916052302635	1.57×10^{-12}
1,298,509	1.00000000033566061	0
1,295,775	1.50000864948046830	1.33×10^{-12}
1,295,774	1.00000000029925395	0
1,161,546	1.49999875722896703	2.78×10^{-12}
1,161,545	1.00000000000617795	0
1,071,949	1.22221480561459564	1.17×10^{-12}
1,071,948	1.30865845687894766	2.60×10^{-12}
1,071,947	1.50000074928158100	1.13×10^{-11}
1,071,946	1.00000000000224576	0
1,000,427	1.81719662622612499	1.06×10^{-12}
1,000,426	1.40245479875694423	2.69×10^{-12}
1,000,425	1.03806026514219285	2.10×10^{-12}
1,000,424	1.85355327456200469	7.74×10^{-12}
1,000,423	1.49999967181406513	2.19×10^{-11}
1,000,422	1.00000000000043077	0
965,071	1.50000537205867124	1.11×10^{-12}
965,070	1.00000000011543611	0
938,447	1.85355385284645369	2.14×10^{-12}
938,446	1.50000130745028737	6.07×10^{-12}
938,445	1.00000000000683764	0
759,772	1.49998970354710015	1.20×10^{-12}
759,771	1.00000000042406767	0
638,119	1.49999574222512311	2.76×10^{-12}
638,118	1.00000000007251466	0
356,629	1.49999038799004736	2.17×10^{-12}
356,628	1.00000000010774093	0
288,949	1.49999038799004736	1.52×10^{-12}
288,948	1.00000000036956282	0
4	1.03806023416757109	4.23×10^{-10}
3	1.85355338902927702	1.56×10^{-9}
2	1.49999999557634922	4.42×10^{-9}
1	1.00000000000000000	0

TABLE VII

Frequency Distribution of Shadowing Errors

Shadowing error intervals	Number of differences $\lvert\bar{C}_2 - \tilde{C}_2\rvert$ falling into interval
1	0
10^{-8}	2
10^{-9}	4
10^{-10}	5
10^{-11}	20
10^{-12}	170
10^{-13}	1843
10^{-14}	18,338
10^{-15}	206,548
10^{-16}	772,226
10^{-17}	331,842
"0"	

to 10^{-12} at the next pre-image step in the vicinity of 1.5. This intermittency is due to the non-uniform Čebyšev measure (2.10b)—or, "density of states"—which has a maximum at 1 and a minimum at 1.5. Iterations that map values of x near 1.5 onto points near 1 evidently increase the density of states; and this enormous compression of images is difficult to simulate with computers that are restricted to shuffling numbers over nearly uniform binary lattices [29]. The overall distribution of shadowing errors is summarized in Table VII. The maximum deviation is 4×10^{-9}. About 99.8% of all the computer elements in this trajectory differ from their analytic counterparts by less then 10^{-14}. As indicated by the last entry in the table, 331,842, or 25%, of the computer iterates are shadowed without any discernible error in double precision.

2.4. A Shadowing Trajectory with 33,732,599 Iterates

Up to this point shadowing trajectories have been constructed starting from well-defined initial elements such as the two members of the quadratic Čebyšev two-cycle shown

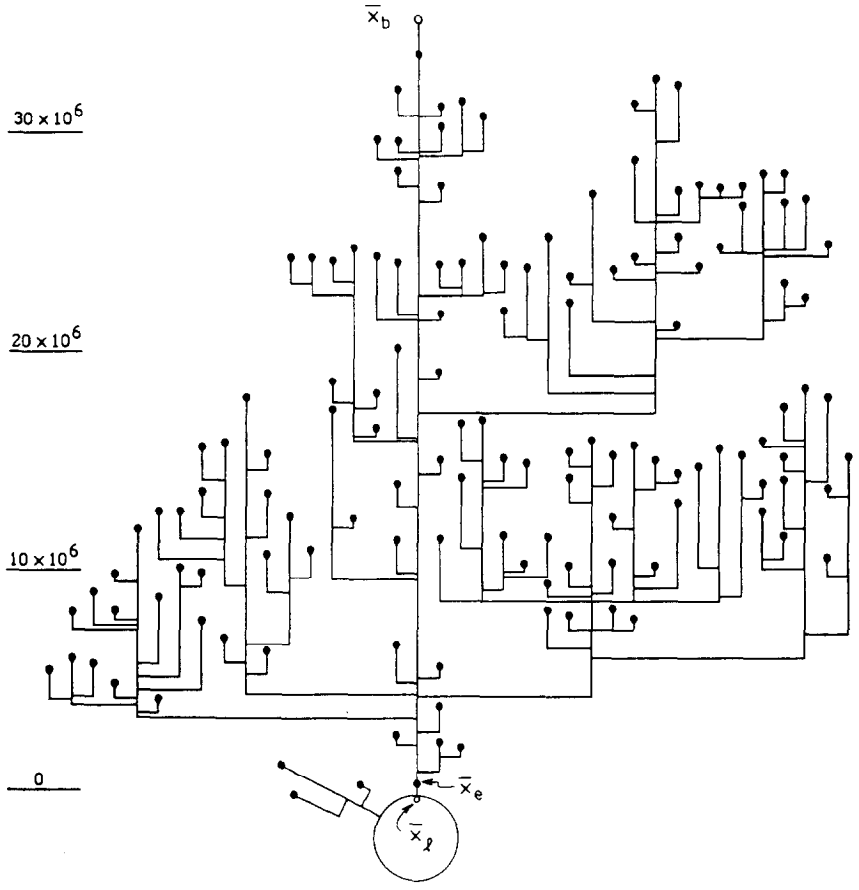

FIG. 4. Dominant computer orbit of the quadratic Čebyšev polynomial. The vertical scale indicates the number of iterations required to reach the terminal loop. The loop itself contains 10,343,527 distinct elements. The 3.3×10^7 element shadowing sequence of Section 2.4 begins at $\bar{x}_b$ and ends at $\bar{x}_e$. The diagram indicates the principal "flow" properties of the trajectories, even though it is only a skeleton representation of the actual computer orbit.

in Fig. 1. This analytic specification appears to be necessary [illegible]

$$\cos\left(\frac{a}{b}\pi\right) \to \cos\left(\frac{2b-a}{2b}\pi\right), \qquad \text{etc.} \tag{2.31}$$

requires specific input values for the constants a and b so that successive shadowing terms can be computed. However, the rapid confluence of the machine iterates $\bar{C}_2$ and the shadowing sequence $\tilde{C}_2$ displayed in Table V suggests that the actual starting point of the shadowing construction is irrelevant. Any element of the form

$$\bar{y}_N = \frac{1}{2}\cos\left(\frac{a_0}{b_0}\pi\right) + \frac{3}{2}, \tag{2.32}$$

with arbitrary initial values satisfying $b_0 \geqslant a_0 > 0$, is suitable as the first term of a shadowing sequence. Let us illustrate this confluence approach with a specific example.

Figure 4 shows several of the longest iteration sequences located by computer explorations of the $\bar{C}_2$ orbit structure. All of these trajectories are part of a dominant orbit that contains approximately 67% of all the computer numbers available in the interval (1, 2)—in VAX double precision this is equivalent to about 2.4×10^{16} distinct elements. Dominant orbits are general features of pseudo-random mappings of finite sets [10, 11, 35]. The fact that most of the trajectories merge into the terminal iterative loop

TABLE VIII

Shadowing Precision for a Trajectory with 33, 732, 599 Iterates

Iterate number	$\bar{C}_2$	$\lvert\delta\rvert$	$\tilde{C}_2$	Shadowing steps
1	1.574 544 548 988 342 31[a]	2×10^{-17}	1.574 ··· 4229	33, 732, 599
2	1.022 227 559 135 501 45	0	1.022 ··· 0145	33, 732, 598
3	1.913 066 020 998 483 11	0	1.913 ··· 8311	33, 732, 597
4	1.682 494 150 814 077 16	5×10^{-17}	1.682 ··· 7711	33, 732, 596
⋮	⋮	⋮	⋮	⋮
33, 732, 536	1.909 895 124 441 912 89	0	1.909 ··· 1289	62
33, 732, 537	1.672 056 052 165 004 97	8×10^{-17}	1.672 ··· 0505	61
33, 732, 538	1.118 413 140 346 427 69	9×10^{-17}	1.118 ··· 2778	60
⋮	⋮	⋮	⋮	⋮
33, 732, 596	1.596 282 627 771 919 54	0.0472 ···	1.549 008 ···[b]	4
33, 732, 597	1.037 081 377 642 663 95	0.0275 ···	1.009 607 ···[c]	3
33, 732, 598	1.857 174 603 700 855 63	0.1048 ···	1.961 939 ···[d]	2
33, 732, 599	1.510 294 790 115 453 09	0.3433 ···	1.853 553 ···[e]	1

[a] This element is part of a set of 27 orphan points.
[b] $\frac{1}{2}\cos(15\pi/32) + \frac{3}{2}$.
[c] $\frac{1}{2}\cos(15\pi/16) + \frac{3}{2}$.
[d] $\frac{1}{2}\cos(\pi/8) + \frac{3}{2}$.
[e] Arbitrary start of shadowing sequence: $\frac{1}{2}\cos(\pi/4) + \frac{3}{2}$.

In Fig. 4, the orphan point $x_b = 1.574\,544\,548\,988\,342\,31$ marks the beginning of a sequence of 33 732 599 computer iterates of $\bar{C}_2$ that leads to the element $\bar{x}_e = 1.510\,294\,790\,115\,453\,09$. The dominant entry point to the loop—indicated by $\bar{x}_l$ in Fig. 4—is only two iterative steps removed at $\bar{x}_l = \bar{C}_2^2(\bar{x}_e) = 1.998\,304\,995\,613\,000\,57$; but it is slightly more convenient to start the shadowing at $\bar{x}_e$. Let us begin by listing the approximate values of $\bar{x}_e$ and its two preceding iterates:

$$\begin{aligned} \bar{x}_{e-2} &\simeq 1.037 \\ \bar{x}_{e-1} &\simeq 1.857 \\ \bar{x}_e &\simeq 1.510. \end{aligned} \tag{2.33a}$$

We then choose a simple but arbitrary initial value for (2.32), say, $\frac{1}{2}\cos(\pi/4) + \frac{3}{2}$, and list its ancestors:

$$\begin{array}{lll} & \textit{Reject} & \textit{Accept} \\ 1.990 \simeq \frac{1}{2}\cos\left(\frac{\pi}{16}\right)+\frac{3}{2} & \frac{1}{2}\cos\left(\frac{15\pi}{16}\right)+\frac{3}{2} \simeq 1.010 \equiv y_{N-2} & \\ 1.038 \simeq \frac{1}{2}\cos\left(\frac{7\pi}{8}\right)+\frac{3}{2} & \frac{1}{2}\cos\left(\frac{\pi}{8}\right)+\frac{3}{2} \simeq 1.962 \equiv y_{N-1} & \\ 1.854 \simeq \frac{1}{2}\cos\left(\frac{\pi}{4}\right)+\frac{3}{2} \equiv y_N. & & \end{array} \tag{2.33b}$$

The shadowing recipe indicated in (2.33b) then simply amounts to selecting successive ancestor branches whose values most closely resemble the corresponding iterates in (2.33a). The "accept–reject" choices indicated in (2.33b) show that only two retrodictions are already sufficient to reduce the initial divergence from $|\bar{x}_e - \bar{y}_N| \simeq 0.343$, by a factor of 10, to $|\bar{x}_{e-2} - \bar{y}_{N-2}| \simeq 0.027$. These selective improvements can obviously be programmed for computers by means of the $\tilde{C}_2$ shadowing algorithms in the Appendix. The construction of the shadowing sequence (2.33b) can therefore be continued automatically from the arbitrary starting point $\bar{y}_N$ all the way back to the beginning of the computer iterations at $\bar{x}_b$. Table VIII displays some excerpts from these results—supplementing and extending the data given in Eqs. (2.33a) and (2.33b). The observed confluence of the $\bar{C}_2$ and $\tilde{C}_2$ sequences after approximately 60 shadowing steps is consistent with the Čebyšev spreading estimate (2.11), adapted to VAX double precision.

If shadowing sequences can be constructed starting from arbitrary initial points, then evidently they cannot be

TABLE IX

Confluence of Multiple Shadowing Sequences

Pre-image choice	Shadowing sequence #1	$\lvert\delta\rvert$	$\bar{C}_2$[a]	$\lvert\delta\rvert$	Shadowing sequence #2	Pre-image choice
S	$\frac{1}{2}\cos\left(\frac{144533\pi}{149504}\right)+\frac{3}{2}\approx 1.00270$	0.00003	1.00267	0.00001	$1.00266\approx\frac{1}{2}\cos\left(\frac{1174577\pi}{1214464}\right)+\frac{3}{2}$	S
L	$\frac{1}{2}\cos\left(\frac{4951\pi}{74752}\right)+\frac{3}{2}\approx 1.98921$	0.00010	1.98931	0.00008	$1.98939\approx\frac{1}{2}\cos\left(\frac{39887\pi}{607232}\right)+\frac{3}{2}$	L
L	$\frac{1}{2}\cos\left(\frac{4951\pi}{37376}\right)+\frac{3}{2}\approx 1.95733$	0.00038	1.95771	0.00031	$1.95802\approx\frac{1}{2}\cos\left(\frac{39887\pi}{303616}\right)+\frac{3}{2}$	L
L	$\frac{1}{2}\cos\left(\frac{4951\pi}{18688}\right)+\frac{3}{2}\approx 1.83659$	0.00142	1.83801	0.00111	$1.83912\approx\frac{1}{2}\cos\left(\frac{39887\pi}{151808}\right)+\frac{3}{2}$	L
S	$\frac{1}{2}\cos\left(\frac{4951\pi}{9344}\right)+\frac{3}{2}\approx 1.45317$	0.00385	1.45702	0.00297	$1.45999\approx\frac{1}{2}\cos\left(\frac{39887\pi}{75904}\right)+\frac{3}{2}$	S
S	$\frac{1}{2}\cos\left(\frac{4393\pi}{4672}\right)+\frac{3}{2}\approx 1.00877$	0.00139	1.00738	0.00098	$1.00640\approx\frac{1}{2}\cos\left(\frac{36017\pi}{37952}\right)+\frac{3}{2}$	S
L	$\frac{1}{2}\cos\left(\frac{279\pi}{2336}\right)+\frac{3}{2}\approx 1.96521$	0.00545	1.97066	0.00390	$1.97456\approx\frac{1}{2}\cos\left(\frac{1935\pi}{18976}\right)+\frac{3}{2}$	L
L	$\frac{1}{2}\cos\left(\frac{279\pi}{1168}\right)+\frac{3}{2}\approx 1.86570$	0.02039	1.88609	0.01475	$1.90084\approx\frac{1}{2}\cos\left(\frac{1935\pi}{9488}\right)+\frac{3}{2}$	L
L	$\frac{1}{2}\cos\left(\frac{279\pi}{584}\right)+\frac{3}{2}\approx 1.53494$	0.06134	1.59628	0.04640	$1.64268\approx\frac{1}{2}\cos\left(\frac{1935\pi}{4744}\right)+\frac{3}{2}$	L
S	$\frac{1}{2}\cos\left(\frac{279\pi}{292}\right)+\frac{3}{2}\approx 1.00488$	0.03220	1.03708	0.04436	$1.08144\approx\frac{1}{2}\cos\left(\frac{1935\pi}{2372}\right)+\frac{3}{2}$	S
L	$\frac{1}{2}\cos\left(\frac{13\pi}{146}\right)+\frac{3}{2}\approx 1.98056$	0.12339	1.85717	0.15639	$1.70078\approx\frac{1}{2}\cos\left(\frac{437\pi}{1186}\right)+\frac{3}{2}$	L
	$\frac{1}{2}\cos\left(\frac{13\pi}{73}\right)+\frac{3}{2}\approx 1.92377$	0.41348	1.51029	0.34903	$1.16126\approx\frac{1}{2}\cos\left(\frac{437\pi}{593}\right)+\frac{3}{2}$	

[a] Double precision values of $\bar{C}_2$ are listed in column two of Table VIII.

unique. This non-uniqueness is well known in the Anosov–Bowen shadowing theory [1, 14], but it is instructive to see explicitly how multiple confluences arise in the Čebyšev computer simulations. Table IX illustrates this behavior for two additional shadowing sequences that follow the 33,732,599 iterates of the $\bar{C}_2$ trajectory in Fig. 4. The new starting points, $\cos(\frac{13}{73}\pi)$ and $\cos(\frac{437}{593}\pi,)$, clearly generate ancestral sequences that are analytically distinct from the initial shadowing set in (2.33b). Yet it is apparent from the numerical trends in Table IX that both of the new shadowing sequences converge rapidly towards the computer iterates. Extensive additional data concerning multiple computer shadowing is summarized in Ref. [11].

3. EXTENSIONS

3.1. Multiple Shadowing and Numerical Order

The non-uniqueness of the shadowing constructions leads to several interesting illustrations of the "folk theorem" that the inverses of sensitive functions are insensitive functions. In particular, the chaotic Čebyšev mappings can be reverted to yield computer algorithms whose output is strictly independent of the input! The construction of such "ultra stable" functions is based on two observations: (1) If the multiple shadowing trials in Table IX are extended to 100 arbitrary starts, then in every case complete confluence—within

the ultimate precision of the computer's floating point lattice—is attained with 65 pre-image generations. (2) In all cases, irrespective of the starting points, the shadowing sequences are characterized by *identical* ancestor–branch choices at every pre-image step. This invariance is evident from the two matching "ancestor choice" columns in Table IX. Every "L" entry signifies the choice of the larger pre-image

$$x \to \tfrac{1}{2}(3 + [x-1]^{1/2}) \qquad \text{(L)} \tag{3.1a}$$

and every "S" entry corresponds to the choice of the smaller pre-image

$$x \to \tfrac{1}{2}(3 - [x-1]^{1/2}) \qquad \text{(S)}. \tag{3.1b}$$

As before, all of these choices follow from the basic shadowing rule that at every step the ancestor that minimizes the difference $|\bar{C}_2 - \tilde{C}_2|$ is selected.

The net result of these retrodictive selections is to supply the missing information that is needed to construct the time reversed trajectories, or equivalently, to "run the film backwards." In this respect, both of the mappings

$${}^{\mathrm{L}}C_2^{-1}: x \to \tfrac{1}{2}(3 + [x-1]^{1/2}) \tag{3.2a}$$

and

$${}^{\mathrm{S}}C_2^{-1}: x \to \tfrac{1}{2}(3 - [x-1]^{1/2}) \tag{3.2b}$$

define inverses of the quadratic Čebyšev polynomial C_2. Of course, the domains and ranges of these functions differ, but it is precisely this mismatch that is essential for ultra-stability. The confluence of the shadowing sequences in Tables VIII and IX can then be formally expressed by the ultra-stable algorithm

$$1.909\,895\,124\,441\,912\,89 = U(\bar{y}_{\mathrm{inp}}), \tag{3.3a}$$

where U is a unique composite of 61 inverse mappings selected from (3.2a) and (3.2b), viz.,

$$U = {}^{\mathrm{L}}C_2^{-1} \circ {}^{\mathrm{L}}C_2^{-1} \circ \cdots \circ {}^{\mathrm{L}}C_2^{-1} \circ {}^{\mathrm{S}}C_2^{-1} \circ {}^{\mathrm{L}}C_2^{-1}. \tag{3.3b}$$

The argument $\bar{y}_{\mathrm{inp}}$ in (3.3a) may be identified with the starting point $1.854\cdots$, as in (2.33b); or with $1.923\cdots$, or $1.161\cdots$, as in the bottom row of Table IX; or we may insert practically *any other* double precision computer number in the interval (1, 2). Computer trials indicate that if (3.3b) is extended to 65 mappings, then it is likely that (3.3a) is valid for *all* double precision $\bar{y}_{\mathrm{inp}} \in (1, 2)$.

Since 55 binary bits are sufficient to specify the 18-digit output in (3.3a) and 61 binary bits are encoded in the sequence of L, L, ..., L, S, L selections in (3.3b), it is clear that the map U does not compress information. This redundancy makes it plausible that the L, ..., S, L sequence in (3.3b) can in fact be adjusted so that the resultant U-algorithm can yield *any* pre-assigned output value for *all* input values of $\bar{y}_{\mathrm{inp}}$ in (1, 2). This option is also confirmed by computer trials [11].

The contrast between the instability of the forward images of C_2 and the stability of the pre-image chain U can be summarized concisely in terms of finite differences: If any double precision number $\bar{y}$ is shifted within the interval (1, 2) by increments of the machine $\varepsilon \sim 2^{-55}$, then the corresponding variation in the forward—or "chaos"—direction is scaled by

$$\Delta C_2^{63}(y \pm \varepsilon) \sim \mathcal{O}(10^{17})\varepsilon, \tag{3.4a}$$

whereas in the inverse—or "ordered"—direction the changes are negligible,

$$\Delta U(y \pm \varepsilon) < \mathcal{O}(1)\varepsilon. \tag{3.4b}$$

3.2. Čebyšev Shadowing Hierarchies: Measures of Complexity

The mixing transformations generated by the iteration of the Čebyšev polynomials C_m $(m \geqslant 2)$ have entropy rates and Liapunov characteristics proportional to $\ln m$, and can therefore simulate many statistical features of disordered systems such as dispersal and ergodicity [8, 31]. Nevertheless, quadratic transformations such as the logistic map (1.1), or its Čebyšev conjugate (2.2), are too rudimentary to qualify as generators of "fully developed chaos" [36, 37] because they have too many short-range correlations. It is easy to verify that strings of numbers resulting from the iteration of (1.1) fail practically all of the pseudo-random number generator tests of the Knuth type [38–40]. One obvious way of minimizing these correlations is to exploit the greater complexity of the higher order Čebyšev polynomials. All of the useful asymptotic properties of the mixing iterations are then preserved, but the higher entropy rates attenuate the short-range correlations. For example, a pseudo-random number generator utilizing C_{3125} passes all of the correlation tests considered in [39, 40], as well as a number of more sophisticated cryptographic diagnostics [11, 41].

Since shadowing is related to the mixing entropy through the Čebyšev spreading theorem (2.11), the shadowing of two Čebyšev polynomials with differing degrees provides another measure of their relative complexity. This aspect of shadowing is illustrated in Table X. The column headed $\bar{C}_{500}$ lists excerpts from a series of 249 computer generated iterates of a 500-degree Čebyšev polynomial, beginning with the element $1.799\,417\cdots$, and ending at $1.938\,795\cdots$. The column headed $\tilde{C}_2$ shows a shadowing sequence con-

TABLE X

Shadowing of $\bar{C}_{500}$ by $\bar{C}_2$

Iteration steps	$\bar{C}_{500}$	$\lvert\delta\rvert$	$\bar{C}_2$	Shadowing steps
1	1.799 417	0.453 926	1.645 509	249
2	1.091 294	0.114 812	1.206 107	248
⋮	⋮	⋮	⋮	⋮
243	1.355 003	0.056 365	1.298 638	7
244	1.545 783	0.227 456	1.773 239	6
245	1.185 004	0.124 674	1.060 329	5
246	1.820 444	0.197 633	1.622 810	4
247	1.122 300	0.016 892	1.105 408	3
248	1.615 889	0.046 443	1.662 333	2
249	1.938 795	0.031 876	1.906 919	1

structed from successive choices of the inverse functions (3.2a) and (3.2b): As indicated in the table, the shadowing is started with the element 1.906 919 $\cdots$; and successive pre-images are picked according to the usual rule that the difference $|\bar{C}_{500} - \tilde{C}_2|$ is to be minimized. It is evident that in contrast to the shadowing confluence displayed in Tables VIII and IX—where both the iteration trajectory and the shadowing sequences are generated by a quadratic Čebyšev polynomial—the $\tilde{C}_2$ sequence in Table X cannot follow the fluctuations of the $\bar{C}_{500}$ iterates. The average deviation of the last five shadowing steps, $\langle|\delta|\rangle_{245\text{-}249} \sim 0.169$, is actually greater than the average initial deviation, $\langle|\delta|\rangle_{1\text{-}5} \sim 0.083$; and further computer trials confirm that under these circumstances there is no tendency for a confluence between $\bar{C}_{500}$ and $\tilde{C}_2$. On the other hand, if the rôles of C_{500} and C_2 are interchanged, there is no difficulty in constructing shadowing sequences. As one might intuitively expect, the pre-images of the more complex C_{500} function can easily follow the fluctuations of the simpler C_2 function.

The shadowing of function pairs is a sensitive measure of relative complexity because it relies on the extended interaction of two distinct processes—iteration and pre-image retrodiction. This synergism yields more information concerning the complexity of pseudo-random systems than some conventional statistical indices. For example, the average fluctuation of successive iterates of C_m is given by the *agitation* [8]:

$$\mathscr{A}(m) \equiv \lim_{p \to \infty} \langle |C_m^{p+1}(x) - C_m^p(x)| \rangle_{x \in [1,2]}. \quad (3.5)$$

Computer trials show that this average fluctuation is essentially independent of m; e.g. $\mathscr{A}(2) \simeq 0.414$, and $\mathscr{A}(500) \simeq 0.404$. This simply means that both the C_2 and C_{500} iterate fluctuations do well in simulating random behavior. However, the inherent differences in complexity of these functions are not reflected in the values of $\mathscr{A}(m)$. Finally we note that the rate of confluence in shadowing, and the asymptotic average of the shadowing distance $|\delta|$ provide additional measures of the relative complexity of pairs of pseudo-random functions [11].

3.3. Iteration and Shadowing Sequences for Random Processes

Since the iteration of Čebyšev polynomials generates strings of pseudo-random numbers that can be ranked in order of increasing complexity by shadowing, it is plausible to match Čebyšev iterates with strings of numbers generated by other means as a gauge of their complexity. An interesting special case is the matching of sets of numbers derived from nominally random processes such as lottery drawings or sequences of radiative transitions in a single atom [41]. The shadowing process in these situations yields results equivalent to the Kolmogorov–Chaitin criterion that the information content of a string of random numbers cannot be compressed [42]. This is illustrated by the simple sequence

$$\underset{\text{iteration}}{\longrightarrow}$$
$$1.52 \quad 1.52 \quad 1.64 \quad 1.64 \quad 1.35 \quad 1.13 \quad 1.35 \quad (3.6)$$
$$\underset{\text{shadowing}}{\longleftarrow}$$

which represents the radiative lifetimes of seven successive decays in a single trapped mercury ion. The two digit accuracy of these numbers reflects the current state of experimental technique.

Suppose first we were to try to reproduce this string of numbers by six iterations of a Čebyšev polynomial in *double precision*, matching only the first three digits. Specifically, this means using the initial three experimental digits, 1.52, as an input, and treating the remaining 15 decimal digits of the double precision representation as adjustable parameters, or "hidden variables." Despite this tremendous latitude in the choice of the starting point—10^{15} possibilities in all!—it can be shown that even as complex a pseudo-random function as $\bar{C}_{500}$ *cannot* reproduce the simple sequence in (3.6) by iteration. The underlying reason for this mismatch is evident if (3.6) is rewritten in the form of an iterative array:

$$\begin{array}{ccccccccc} 1.52 & & 1.52 & & 1.64 & & 1.64 & & 1.35 & & 1.13 & & 1.35 \\ \downarrow & & \downarrow & & \downarrow & & \downarrow & & \downarrow & & \downarrow & & \downarrow \\ \bar{x}_0 & & \bar{x}_1 & & \bar{x}_2 & & \bar{x}_3 & & \bar{x}_4 & & \bar{x}_5 & & \bar{x}_6 \\ \downarrow & & \downarrow & & \downarrow & & \downarrow & & \downarrow & & \downarrow & & \\ \bar{x}_0 & \to \bar{C}_{500}(\bar{x}_0) & & & \bar{x}_2 & \to \bar{C}_{500}(\bar{x}_2) & & & \bar{x}_4 & \to \bar{C}_{500}(\bar{x}_4) & & & \end{array} \quad (3.7a)\ (3.7b)\ (3.7c)$$

Clearly, if the numbers in (3.7a) really did correspond to

iterates of $\bar{C}_{\ldots}$ then (3.7b) and (3.7c) show that successive tions, shadowing results of this type apply to *all* elements of

points on the graph of $\bar{C}_{500}$. The fact that the series (3.7a) mations. Since the Čebyšev polynomials are conjugate to cannot be approximated by iterates of $\bar{C}_{500}$ simply means that this geometric criterion is not satisfied, or, equivalently, that $\bar{C}_{500}$ fails the serial correlation test [38].

Of course, the series in (3.6) can be reproduced by resorting to still more complicated iterations. For instance, if the graph of $\bar{C}_{10000}$ is plotted in the unit square, and this is overlaid with a uniform 100×100 square grid, then the 10,000 oscillations of $\bar{C}_{10000}$ are sufficiently fine so that the graph will intersect every individual square of the grid. Consequently, every possible pair of two-digit numbers will approximate some point on the graph of $\bar{C}_{10000}$; or, at this level of precision, $\bar{C}_{10000}$ will pass the serial correlation test and simulate (3.6).

The Kolmogorov–Chaitin randomness criteria enter if we try to simulate the experimental series (3.6) by shadowing rather than iteration. In this case we take the last entry, 1.35, as the starting point, and construct shadowing sequences following the methods outlined in Section 2.4 and the Appendix. In particular, if we elect to shadow with C_{500}, then all seven numbers in (3.6) can easily be reproduced by analytical expressions: This is simply due to the fact that every C_{500} iterate has 500 distinct pre-images distributed throughout the interval $[1, 2]$ with the Čebyšev measure (2.9); and therefore the number 1.13—the entry preceding 1.35 in (3.6)—is sure to be approximated to better than 1% precision by one of the pre-images of 1.35. Similar arguments apply to all the remaining entries in (3.6); and in this sense it is feasible to shadow the random experimental results in (3.6) by deterministic algorithms.

Since shadowing is based on retrodiction, this scheme can neither compress information nor predict new results for genuinely random sequences. The experimental information is simply transcribed into a pre-image selection sequence analogous to the "L–S" coding in (3.3b). Clearly, this is just another restatement of the Kolmogorov–Chaitin randomness criterion [42].

4. SUMMARY: PHYSICAL IMPLICATIONS

4.1. Summary of Results

4.1.1. *Correct Numbers versus Arbitrary Numbers.*

The basic conclusion that emerges from the shadowing studies is that the computer iteration of chaotic functions can yield trajectories that closely approximate portions of the exact orbits despite the cumulative growth of roundoff and truncation errors. The net effect of the machine perturbations is simply to shift the computed sequence of values from the vicinity of one exact trajectory to the proximity of another exact trajectory. Apart from a few isolated exceptent maps, some logistic transformations, and are also related to other classes of functions such as quantum mechanical probability distributions [43], these shadowing results have a general significance.

In the particular case of Čebyšev iterations, the existence of shadowing sequences can be established by several methods. For example, the analytic structure of simple orbits, such as the set of all C_2 iterates that terminate in a two-cycle, can be determined explicitly; and it is then feasible to check directly to what extent the computer generated iterates can reproduce this structure. Alternatively, a complex machine generated orbit such as the dominant $\bar{C}_2$ orbit depicted in Fig. 4, may be regarded as the given structure; and shadowing then consists of verifying that every trajectory of this machine orbit can in fact be approximated by sequences of exact C_2 pre-images constructed with the help of the retrodictive algorithms of Section 2.4 and the Appendix.

Of course computer simulations can go astray if the roundoff and truncation errors become too large. For instance, the step-wise perturbations, δ_j in (1.17a), can be magnified in a controlled way by deliberately throttling the accuracy of the computers' arithmetic. Extensive trials with variable precision computations demonstrate that the Čebyšev iterations become severely distorted when the rate of growth of the roundoff errors dominates the intrinsic mixing rate (Section 5 of Ref. [8]). Under these circumstances, shadowing will fail because the computed values of the iterates are not merely shifted from one "correct" Čebyšev sequence to another, but are only weakly correlated with the algorithms that are programmed on the machine. In this respect, amplified computer noise can produce effects analogous to those that prevent the simple C_2 algorithm from shadowing the more complex C_{500} iterates.

4.1.2. *Shadowing and Orbit Structures*

Even though an entire computer generated orbit—such as the one shown in Fig. 4—may be closely shadowed by a set of exact trajectories; the numerical match does not imply any generic correspondence between the analytic orbit structure and the orbits of the computer simulations. These differences arise from the finite nature of the machine computations and the fact that the shadowing sequences are constructed by entirely different means than the iterative trajectories that they numerically follow.

For example, the most prominent features of the iterative computer network in Fig. 4 are: (i) the existence of initial or "orphan" points that constitute the sources for all machine generated trajectories; (ii) the marked tendency for all trajectories to merge into larger "river basins"; and (iii) the

iterative "clock," or terminal loop, that is the canonical end state for all iterative processes on finite sets. General combinatorial arguments show that deterministic simulations of random processes on finite sets, as well as randomly chosen mappings of finite sets, generate precisely these types of orbits [11, 13, 35]. In this respect, the computer implementation of the Čebyšev iterations yield reliable and quantitatively correct results. Furthermore, the Čebyšev simulations have the shadowing property. But clearly the inference that shadowing also validates the computer modeling of the exact analytic Čebyšev orbits is unwarranted and misleading.

The principal differences between computer shadowing and iterative processes are illustrated in Table XI. This example shows what happens when portions of a trajectory, such as the 18-element segment marked in Fig. 2, are traversed three times by two different computational schemes. First, the column headed "iteration sequence # 1" lists the successive numerical values obtained when the machine algorithm, $\bar{C}_2$ of (2.14), is iterated by means of the recursion relation (2.16). This sequence of iterates merges into the computer two-cycle, $\bar{C}_2^2(\bar{x}_{1U}) = \bar{x}_{1U}$, depicted in Fig. 2. Every element of this sequence also satisfies a numerical consistency condition: if $\bar{x}_{j-1}$ and $\bar{x}_j$ are two successive elements, then $\bar{x}_{j-1}$ must be part of the pre-image fan of $\bar{x}_j$, cf. (2.20a); and $\bar{x}_j$ in turn must be the computer generated iterate of $\bar{x}_{j-1}$.

The second traverse of the segment $x_{1U} - x_{17}$, by means of shadowing methods, yields the numbers listed in the column under "shadowing sequence." All of these values are derived from the analytic and numerical results summarized in Table I. Clearly, the iteration and shadowing elements deviate at most by 1.3×10^{-16}, and both sequences merge into the C_2 two-cycle. But the shadowing elements are not constrained by any numerical consistency conditions. Consequently, a third traverse of this segment with a new series of iterations can yield completely different results. The column headed "iteration sequence # 2" in Table XI shows the computer output when another iteration is started at the "exact" shadowing value $x_{17} \to 1.38\cdots110$, instead of at the old "inexact" value $1.38\cdots104$. Evidently the $\bar{C}_2'$ iterations deviate rapidly both from the original $\bar{C}_2$ iterations, as well as the $\tilde{C}_2$ shadowing elements. In fact, $\bar{C}_2'$ does not even belong to the same computer orbit! Instead of converging towards the C_2 two-cycle, the $\bar{C}_2'$ trajectory merges into the terminal loop of the dominant $\bar{C}_2$ orbit in Fig. 4 after 8, 114, 611 iterations.

TABLE XI

Differences between Shadowing and Iteration Sequences

Label of point in Fig. 2	$\bar{C}_2$ iteration sequence # 1	$\tilde{C}_2$ shadowing sequence	$\bar{C}_2'$ iteration sequence # 2
17	1.38···104	1.38···110	1.38···110
16	1.04···650	1.04···647	1.04···628
15	1.81···312	1.81···320	1.81···379
14	1.39···033	1.39···1046	1.39···1188
13	1.04···766	1.04···4776	1.04···4643
12	1.83···399	1.83···2396	1.83···2865
11	1.43···195	1.43···93203	1.43···94439
10	1.01···102	1.01···59105	1.01···58480
9	1.93···146	1.93···019146	1.93···021566
8	1.77···833	1.77···439828	1.77···448337
7	1.29···960	1.29···842952	1.29···861590
6	1.16···905	1.16···335914	1.16···323040
x_{54U}	1.46···759	1.46···607754	1.46···688850
x_{42U}	1.00···111	1.00···243114	1.00···217665
x_{31U}	1.97···682	1.97···457679	1.97···858224
x_{2U}	1.90···373	1.90···747373	1.90···129867
x_{1U}	1.65···373	1.65···747373	1.65···985160

Of course, this behavior does not imply that the numbers generated by $\bar{C}_2$ and $\tilde{C}_2$ are in any sense more exact or "correct." There is no difficulty in constructing still other shadowing sequences that closely track $\bar{C}_2'$ to validate its numerical and structural properties. The essential point is that behind the scrim of numerical resemblance, computer shadowing and iteration are inherently different processes.

4.1.3. *Shadowing and Statistical Properties*

Computer simulations of chaotic systems are frequently used to generate statistical information concerning their average behavior. For instance, in their pioneering investigations of energy exchange in complex systems, Fermi, Pasta, and Ulam modeled the non-linear coupling of sets of oscillators on computers and inferred the non-ergodic evolution of the energy distribution by statistical sampling of the numerical solutions [44]. In contrast, mixing systems such as billiards in a stadium or Čebyšev iterations are ergodic, and this property is also reflected in computer simulations. Nevertheless, there are no general results that guarantee the validity of computer generated statistics for these kinds of systems.

It has been argued that at least in those cases where the computer models of chaotic systems have the shadowing property, there is an *a priori* assurance that sampling the numerical orbits does yield the correct statistics for the actual systems [14]. But this argument has a gap. Consider, for example, the C_2 shadowing sequence in (3.3b):

$$U = {}^{L}C_2^{-1} \circ {}^{L}C_2^{-1} \circ \cdots \circ {}^{L}C_2^{-1} \circ {}^{S}C_2^{-1} \circ {}^{L}C_2^{-1}. \quad (4.1)$$

Since this expression is the numerical approximation for a simple deterministic process—the C_2 iterations—implemented by a specific program on a particular computer, the entire chain of ${}^{L}C_2^{-1}$, ${}^{S}C_2^{-1}$ functions in (4.1) is, in principle, completely determined for every trajectory in all the computer orbits. But then, why is it necessary to resort to

interval arithmetic experiments [3, 4], or to step-by-step retrodictions in order to verify the existence of shadowing trajectories? Clearly, the reason is that the theory of computer arithmetic is not yet sufficiently developed so that one can dispense with the numerical trials [29]. We do not even have any direct tests that distinguish between orphan points and interior points in computer orbits.

The only conclusion that is justified by shadowing sequences such as (4.1) is that the numbers generated by computer iterations are not arbitrary, but approximate the elements of an exact trajectory. However, this still does not guarantee the statistical fidelity of the simulations. The statistics depend on the actual distribution of values along the computer trajectories, and these, in turn, are encoded by the specific sequence of ${}^{\mathrm{L}}C_2^{-1}$ and ${}^{\mathrm{S}}C_2^{-1}$ functions in shadowing expressions such as (4.1). Since these L, S, ... patterns cannot be predicted by any current methods, both shadowing and statistical properties have to be established by empirical computer trials.

4.2. Physical Implications

The iteration of the Čebyšev polynomials can be modeled by physical systems as well as by digital computer simulations. For instance, the mapping $x \to x^2 - 2$ can be reproduced by voltage variations in analogue computer elements such as biased product detectors [28]; and the trigonometric representation of the iterates,

$$C_2^p(x) = \cos(2^p \cos^{-1} x) \tag{4.2}$$

can be modeled by sets of gears linked together to form a "logarithmic clock" [45]. Each of these physical devices highlights special features of the Čebyšev iterations. For example, the Čebyšev polynomials form a semi-group under composition,

$$C_n^p \circ C_n^q = C_n^{p+q}, \qquad p, q = 1, 2, ..., \tag{4.3}$$

but it is not possible to extend (4.3) to non-integral values of p and q [9]. Consequently, the Čebyšev polynomials cannot be embedded in a flow; and, in particular, $C_2(x)$ has no fractional iterates whatsoever [46]. Physically this means that any voltage transducer with the property that

$$V(\text{output}) = [V(\text{input})]^2 - 2 \tag{4.4}$$

is an irreducible circuit element in the sense that it cannot be replaced by two other identical transducers that generate the voltage transformation (4.4) when connected in cascade. The fact that there is no flow that assigns values "in between" the iterates $C_2^p(x)$ and $C_2^{p+1}(x)$ also implies that the Čebyšev trajectories cannot be derived from Hamiltonian dynamics. In general, functions can be embedded in flows—or continuous iteration semi-groups—only if their iterative structures satisfy highly restrictive compatibility conditions. For example, every function in a one-dimensional flow with continuous trajectories must be non-decreasing; consequently such flows are not suitable for describing chaotic systems [47]. On the other hand, the baker's transformation—which is a two-dimensional mixing transformation suitable for modeling chaotic behavior—is not embeddable in a flow [48]. These examples illustrate the assertions of Poincaré and Krylov that the description of disordered systems lies outside the scope of Hamiltonian dynamics [49, 50].

The logarithmic clock model shows that it is feasible to combine smooth evolution with the Čebyšev iterations by interpolating between the iterates $C_2^p(x)$ and $C_2^{p+1}(x)$ in a physically reasonable way. This construction does not conflict with any of the preceding results because the discrete Čebyšev iterates are embedded in continuous *higher dimensional* trajectories. There are also abstract methods for associating discrete n-dimensional mappings with differentiable trajectories in $(2n+1)$-dimensional spaces [51]. In the case of the mechanical gear model, the smooth evolution has been secured at a price. As shown in [45], the logarithmic clock trajectory is a three-dimensional variable pitch helix—a differentiable curve without any chaotic filigrees. Evidently, the embedding has not only "smoothed" the Čebyšev trajectories, it has also obliterated all of their pseudo-random properties. Conversely, this example demonstrates how the mixing properties of the Čebyšev iterations arise from the selective omission of information and the illusion of dimensional reduction.

The connections between physical and abstract models of chaotic systems also affect the physical interpretation of various ergodic theorems: (1) For instance, if ergodicity is identified with metric transitivity, then it is well known that Hamiltonian flows can never be ergodic [23]. An elementary corollary is that the trajectories of the logistic map (1.1) are not derivable from Hamiltonian mechanics. (2) Ergodicity is also incompatible with Hamiltonian mechanics if it is interpreted in the original (Boltzmann) sense of systems that wander everywhere in phase space. Trajectories that are derivable from Hamiltonian mechanics can not reach everywhere in phase space because of measure-theoretic restrictions [52]. And if they do reach everywhere, the trajectories would have to be space-filling non-differentiable curves (e.g., Peano curves) that could not qualify as Hamiltonian trajectories [53]. (3) The subtle physical relation between ergodicity and embeddability is also illustrated by the following results: The ergodic automorphisms of an n-dimensional torus are not embeddable in a flow [54]. However, these automorphisms can always be suspended in a one-way flow. There is no contradiction, because "embedding" and "suspending" refer to two distinct technical constructions. Suspension is more flexible because it is somewhat analogous to interpolating trajectories in higher dimensional spaces as in the clock

example. (4) Geodesic flows on closed surfaces with negative curvature are ergodic [1, 55]. This result may have physical implications because it is plausible to identify these flows with the dynamics of an object constrained to move on a surface with a metric that has negative curvature everywhere. However, a straightforward realization is impossible because closed surfaces with negative curvature cannot be isometrically embedded in three-dimensional Euclidean space. One way of circumventing this difficulty with a physical arrangement was suggested by Kolmogorov [56]; but subsequent work still has not led to any conclusive results [57].

A close correspondence between computer simulations and chaotic physical systems prevails in cases where the evolution is described by strings of pseudo-random numbers. Ferromagnets are a representative example. In these systems, the response to variations of an external magnetic field consists of a wandering through a tremendous multiplicity of metastable states—each corresponding to a locally stable configuration of the magnetic domain structure. In principle, this evolution is deterministic—especially in macroscopic systems where quantum effects are irrelevant—but of course it is history dependent and extremely sensitive to initial conditions. Pseudo-random computer simulations can be used to model these hysteresis effects [18]. In fact, since the computers themselves are complex switching networks with many states or displays, this correspondence is really not a simulation, but rather a comparison of two physical systems with analogous properties. Schematically,

$$\text{ferromagnet} \leftrightarrow \text{computer} + \text{pseudo-random number algorithm}.$$

This simple equivalence suggests a broader perspective on the role of computers in statistical physics. For example, instead of regarding the differences between the "correct" orbit in Fig. 1 and the "incorrect" orbit in Fig. 2 as annoying distortions introduced by computer roundoff and truncation errors, it is also possible to consider the trajectories in Fig. 2 as interesting manifestations of a new symmetry breaking mechanism latent in complex switching networks. A similar emphasis on the physical aspect of computing has already yielded useful results concerning energy dissipation and information processing [58]. Further studies of the physical properties of complex switching networks are likely to be fruitful.

APPENDIX: THE $\tilde{C}_2$ ALGORITHM

The construction of shadowing sequences requires the numerical evaluation of pre-image relations involving $\cos(A\pi/B)$, where A and B may be very large numbers. In particular, Eqs. (2.7a)–(2.8) imply that both the numerator and denominator of the cosine's argument increase monotonically with successive pre-images. Unchecked, this monotonic growth would quickly result in arithmetic overflow. This is avoided by dividing the numerator by a common factor as soon as the denominator reaches a critical size, viz.

$$\frac{N\times 10^{m+n}}{D\times 10^{m+d}} \Rightarrow \frac{N\times 10^{n}}{D\times 10^{d}}, \quad \text{when} \quad m+d>500,\ m=450. \tag{A.1}$$

Because of the limited computer memory, the values of the numerator and denominator eventually exceed the available storage capacity. However, in virtue of the monotonic growth, the most significant digits can be determined with adequate precision. Typically, if the exact pre-image is

$$\frac{1}{2}\cos\left(\frac{A\pi}{B}\right)+\frac{3}{2}, \qquad A\gg 1,\ B\gg 1,\ B>A, \tag{A.2}$$

then the machine representation is equivalent to

$$\frac{1}{2}\cos\left(\frac{A+a}{B+b}\pi\right)+\frac{3}{2}, \qquad A\gg a,\ B\gg b,\ B+b>A+a, \tag{A.3}$$

where a and b are digits that will be lost because of the computer's limited memory. The difference between (A.2) and (A.3) is bounded by a term of order $\text{Max}\{a/B, b/A\}$. Therefore, if all of the pre-images are computed in quadruple precision, the error will be of the order of 10^{-30}. This is an adequate margin of safety for 10^7 iterations accurate to double precision.

ACKNOWLEDGMENTS

We thank M. J. Frank, E. T. Olsen, and A. Sklar for many helpful conversations and critical remarks. It is also a pleasure to acknowledge the support of the Research Corporation. D.G. is grateful to the Sante Fe Institute for the award of a summer fellowship.

REFERENCES

1. D. V. Anosov, *Proc. Steklov Inst. Math.* **90** (1967).
2. R. Bowen, *J. Differential Eq.* **18**, 333 (1975).
3. S. M. Hammel, J. A. Yorke, and C. Grebogi, *J. Complexity* **3**, 136 (1987).
4. S. M. Hammel, J. A. Yorke, and C. Grebogi, *Bull. Amer. Math. Soc.* **19**, 465 (1988).
5. R. M. May, *Nature* **261**, 459 (1976).
6. P. Collet and J. P. Eckmann, *Iterated Maps on the Interval as Dynamical Systems* (Birkhauser, Boston, 1980).

7. R. L. Adler and T. J. Rivlin, *Proc. Amer. Math. Soc.* **15**, 794 (1964).
8. T. Erber, P. Everett, and P. W. Johnson, *J. Comput. Phys.* **32**, 168 (1979).
9. P. Johnson and A. Sklar, *J. Math. Anal. Appl.* **54**, 752 (1976).
10. T. Erber, T. M. Rynne, W. F. Darsow, and M. J. Frank, *J. Comput. Phys.* **49**, 394 (1983).
11. D. Gavelek, *Computer Orbits of Čebyšev Mixing Transformations*, Ph.D. thesis, Illinois Institute of Technology, Chicago, 1990.
32. E. M. Coven, I. Kan, and J. A. Yorke, *Trans. Am. Math. Soc.* **308**, 227 (1988).
33. R. E. Rice, *Aequationes Math.* **17**, 104 (1978).
34. A. Sklar, private communication.
35. P. Flajolet and A. M. Odlyzko, in *Advances in Cryptology: Eurocrypt '89*, edited by J. J. Quisquater, Lecture Notes in Computer Science, 434 (Springer-Verlag, New York/Berlin, 1990), p. 329.
36. J. Gleick, *Chaos, Making a New Science* (Penguin, New York, 1988).

481 (1983).
13. T. Erber, W. F. Darsow, M. J. Frank, and D. Gavelek, to be published.
14. G. Benettin, M. Casartelli, L. Galgani, A. Giorgilli, and J.-M. Strelcyn, *Nuovo Cimento B* **44**, 183 (1978).
15. A. M. Liapunov, *Stability of Motion* (Academic Press, New York, 1966).
16. W. Hahn, *Stability of Motion* (Springer-Verlag, New York, 1967).
17. F. C. Moon, *Chaotic Vibrations* (Wiley, New York, 1987).
18. T. Erber and S. A. Guralnick, *Ann. Phys. (N.Y.)* **181**, 25 (1988).
19. F. M. Penning, *Physica* **3**, 873 (1936).
20. C. Lanczos, *The Variational Principles of Mechanics*, Univ. of Toronto Press, Toronto, 1966.
21. O. E. Lanford III, in *Chaotic Behavior in Deterministic Systems*, edited by G. Iooss, R. H. G. Helleman, and R. Stora (North-Holland, Amsterdam, 1983), p. 73.
22. Y. Choquet-Bruhat and C. DeWitt-Morette, *Analysis, Manifolds and Physics* (North-Holland, Amsterdam, 1982).
23. V. I. Arnold and A. Avez, *Ergodic Problems of Classical Mechanics* (Benjamin, New York, 1968).
24. J. I. Palmore and J. L. McCauley, *Phys. Lett. A* **122**, 399 (1987).
25. T. Erber, B. Schweizer, and A. Sklar, *Commun. Math. Phys.* **29**, 311 (1973).
26. T. Erber and P. Johnson, *Bull. Am. Phys. Soc. II* **19**, 41 (1974).
27. B. Schweizer and A. Sklar, *Probabilistic Metric Spaces*, (North Holland, New York, 1983).
28. T. Erber and A. Sklar, in *Modern Developments in Thermodynamics*, edited by B. Gal-Or (Wiley, New York, 1974), p. 281.
29. U. W. Kulisch and W. L. Miranker, *SIAM Rev.* **28**, 1 (1986).
30. H. Brolin, *Arkiv. Mat.* **6**, 103 (1965).
31. R. L. Adler, A. G. Konheim, and M. H. McAndrew, *Trans. Am. Math Soc.* **114**, 309 (1965).
38. D. E. Knuth, *The Art of Computer Programming, Vol. 2, Seminumerical Algorithms*, 2nd ed. (Addison–Wesley, Reading, MA, 1981).
39. J. M. Hosack, *J. Comput. Phys.* **67**, 482 (1986).
40. R. S. Wikramaratna, *J. Comput. Phys.* **83**, 16 (1989).
41. T. Erber, P. Hammerling, G. Hockney, M. Porrati, and S. Putterman, *Ann. Phys. (N.Y.)* **190**, 254 (1989).
42. G. J. Chaitin, *J. Assoc. Comput. Mach.* **21**, 403 (1974).
43. T. Erber, T. M. Rynne, and A. Sklar, *Acta Phys. Austriaca* **53**, 145 (1981).
44. E. Fermi, J. Pasta, and S. Ulam, in *Enrico Fermi: Collected Papers*, Vol. II (Univ. of Chicago Press, Chicago, 1965), p. 978.
45. T. Erber, P. Johnson, and P. Everett, *Phys. Lett. A* **85**, 61 (1981).
46. R. E. Rice, B. Schweizer, and A. Sklar, *Am. Math. Monthly* **87**, 252 (1980).
47. A. Sklar, *Radovi Math.* **3**, 111 (1987).
48. B. Schweizer and A. Sklar, *Found. Phys.* **20**, 873 (1990).
49. H. Poincaré, *C. R. Acad. Sci. Paris* **108**, 550 (1889).
50. N. S. Krylov, *Works on the Foundations of Statistical Physics* (Princeton Univ. Press, Princeton, NJ, 1979).
51. N. P. Zidkov, *Mosk. Gos. Univ. Uc. Zap.* **163**, 31 (1952).
52. M. Plancherel, *Ann. Phys. (Leipzig)* **42**, 1061 (1913).
53. A. Rosenthal, *Ann. Phys. (Leipzig)* **42**, 796 (1913).
54. K. Ghebremeskel and A. Sklar, in preparation.
55. E. Hopf, *Ber. Verh. Saechs. Akad. Wiss. Leipzig* **91**, 261 (1939).
56. A. N. Kolmogorov, Intern. Congr. Math. 1954; reprinted in *Foundations of Mechanics*, R. Abraham and J. E. Marsden (Benjamin, New York, 1967), Appendix D.
57. N. Abe, *Adv. Stud. Pure Math.* **3**, 87 (1984).
58. R. Landauer, *Nature* **335**, 779 (1988).